ABSTRACT

Title of Thesis: INVESTIGATION OF THE IMPACT OF ACOUSTIC FORCING ON NEURAL NETWORK ACTIVITY

Arijit Dutta, Master of Science, 2024

Thesis Directed By: Dr. Wolfgang Losert, Fischell Department of Bioengineering

The increase in the prevalence of neurological disorders, now approximated to affect 15% of the worldwide population, has highlighted the need to fundamentally understand how neuronal networks function in normal and diseased conditions. Acoustic forcing has been identified as a method to advance the fabrication and understanding of how neural networks function via cell patterning and neuromodulation. This phenomenon occurs as acoustic waves at ultrasonic frequencies impart a force on a target through a medium. Cell patterning via acoustic forcing has led to the development of biomimetic neural organoids. Neuromodulation, via acoustic forcing, has been shown to stimulate neuronal activity and is popularly researched in transcranial focused ultrasound. A concern in transcranial focused ultrasound is standing wave formation, and thus pressure gradients, in the brain. The mechanism of how standing wave formation impacts neuronal network activity remains unknown. This thesis elucidates the impact of acoustic standing waves on large-scale neuronal activity through the fabrication and application of a standing-wave generating device on assembled ReNcell human neural progenitor-derived neural networks. The preliminary results showed younger networks to have large decreases in activity while older networks saw minimal change following acoustic forcing application. Additionally, varying intensity from did not affect network activity of older networks during acoustic forcing application.

INVESTIGATION OF THE IMPACT OF ACOUSTIC FORCING ON NEURAL NETWORK ACTIVITY

by

Arijit Dutta

Thesis submitted to the Faculty of the Graduate School of the
University of Maryland, College Park, in partial fulfillment
of the requirements for the degree of
Master of Science
2024

Advisory Committee:
Professor Wolfgang Losert, Chair
Professor John P Fisher
Professor William Bentley

Acknowledgements

I would like to thank Dr. Losert for giving me the opportunity to carry out my thesis work in his lab and for his guidance throughout the project. I would also like to thank the members of the Losert lab for welcoming me into the lab, training me on the lab equipment, and providing feedback on my thesis work. Lastly, I would like to thank my family and friends in the Bioengineering department for their support and guidance on my thesis work.

Table of Contents

List of Tables

List of Figures

Chapter 1: Introduction

Ultrasound has been an ever increasingly used technology since its initial discovery decades ago. Aside from its commonly known use in diagnostic imaging, ultrasound usage has expanded to therapeutic applications such as thermal ablation, drug delivery, and for the purpose of this thesis, neuromodulation.

The principal idea upon which ultrasound technology is based is the utilization of high frequency waves with frequencies greater than 20 kHz[1]. These waves are sinusoidal fluctuations in pressure[2]. This frequency range is beyond what the range that is audible to the human ear. Acoustic forcing is the phenomenon in which ultrasonic acoustic waves propagate within a medium to exert force on an object[3]. In the context of bioengineering, acoustic forcing has many uses that have contributed significantly to the advancement of the field.

The emphasis of this thesis is on acoustic forcing in the scope of neural tissue formation and stimulation. It is approximated that approximately 15% of the worldwide population have some type of neurological disorder[4]. This highlights the need to understand how neurological systems function and define better treatments. Acoustic forcing has been used in producing neural constructs and in neuromodulation. This thesis focuses on elucidating the impact of acoustic forcing, via standing acoustic waves, on neural network activity. Standing acoustic waves have already been used in neuronal cell patterning but its effect on the cell signaling activity remains understudied. This is important to understand because standing wave formation can occur in transcranial focused ultrasound-based neuromodulation and

create potentially dangerous pressure gradients within the brain[5]. Thus, to continue the development of ultrasound usage in therapeutic use cases, the impact of standing waves on neuronal activity needs to be understood.

The outline of this thesis is the following: the second chapter discusses the various applications of acoustic forcing in the bioengineering field; the third details the fundamental theory behind acoustic forcing; the fourth and final chapter describes my investigation into the impact of standing wave based acoustic forcing on neural network activity.

Chapter 2: Acoustic Forcing in Bioengineering

This chapter describes the variety of applications of acoustic forcing in bioengineering. It will show how multi-faceted this phenomenon can be in its applications in the bioengineering field. The specific areas of bioengineering discussed include tissue engineering, lab-on-chip devices, and drug delivery.

2.1 Acoustic Forcing in Tissue Engineering

Tissue engineering is a sub-discipline of bioengineering that focuses on the integration of material science and cell biology with a desired goal of maintaining or restoring tissue function[6]. The tissue engineering scope is a vast encompassing field ranging from 3D tissue printing to cell patterning to stem cell differentiation. Acoustic forcing has been investigated as a technique to improve bioprinting, cell patterning, and cell differentiation work.

2.1.1 Bioprinting

One of the main facets of tissue engineering currently being developed and used is 3D bioprinting. The basis of this technology is to develop biomimetic structures that can be used in restorative purposes for regenerative medicine or as a model platform for testing novel therapies[37]. The popular printing techniques used in bioprinting include ink-jet, extrusion-based, and laser-assisted bioprinting[8]. The main considerations to account for while selecting a bioprinting technique are resolution and post-print cell viability.

In inkjet based bioprinting, a portion of the bio ink is heated up to form a droplet and is dropped onto the printing bed. This can be done via thermal or piezoelectric drop-on-demand methodology. As seen in Figure 1 provided by Agarwal et al, both methods dispense the bio ink in droplet form onto the substrate[9]. The thermal method vaporizes ink droplets which form vapor bubbles that push out another droplet onto the substrate through the nozzle. The piezoelectric method uses pulsed voltage to stimulate the transducers which then create pressure to push out droplets of the bioink.

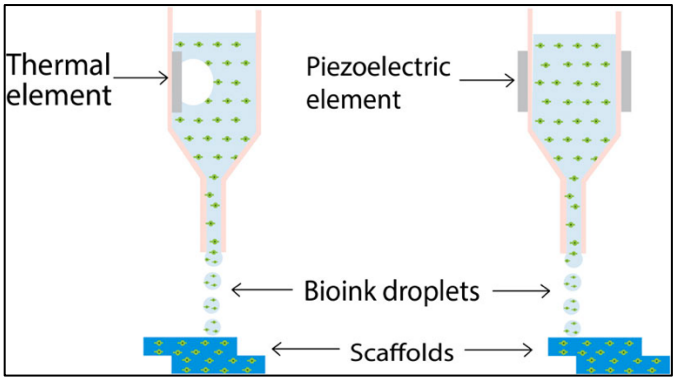

Figure 1. Illustrations, by Agarwal et al, of how acoustic forcing is used in inkjet-based 3D printing. The left side is the thermal based method, and the right is via piezoelectric method[9].

One of the main issues with the above-mentioned printing methods is the use of a nozzle. This nozzle use requires the utilized bio ink to have a limited cell density and its diameter impacts the print resolution and viability. A larger nozzle diameter exerts less pressure on the cell-laden ink but is limited to smaller resolution while a smaller nozzle diameter exerts a larger shear stress, which can negatively impact cell viability, but has a larger resolution[10]. Acoustic droplet ejection (ADE) is a relatively new bioprinting methodology that circumvents the need and issues associated with nozzle-based inkjet bioprinting. While the specifics of an ADE based printer may differ from printer to printer, the principal idea remains the same: ultrasound waves emitted from a piezoelectric crystal are directed at a specific point in the printing material via a coupling medium such as water. If the ultrasound energy is greater than the surface tension of the liquid, a droplet is emitted onto the printing plate[11]. A diagram of the idea of ADE is shown in Figure 2. The droplet size can be modulated from micron to millimeter scale based on the frequency used with higher frequencies creating smaller droplets[11].

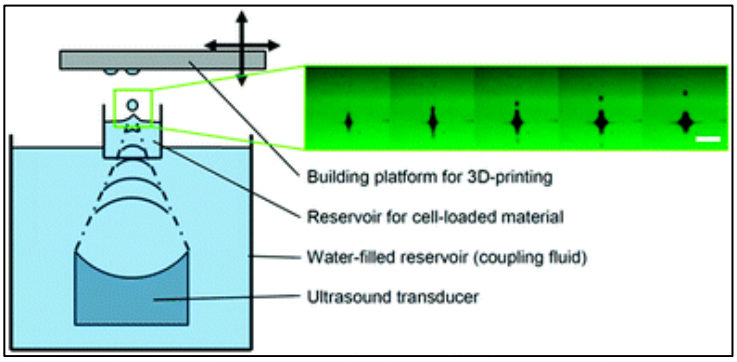

Figure 2. Schematic depicting how acoustic droplet ejection printing utilizes acoustic forcing[11].

2.1.2 Cell Patterning

The microarchitecture of certain tissue systems, such as neuronal or vasculature systems, are very complex and difficult to recapitulate accurately in an in

vitro setting. Bioprinting with traditional 3D techniques have been used in this manner but suffer from inaccuracy in proper recapitulation of the target tissue.

Neuron based organoids, such as the cerebral cortex, are a particularly difficult model type to print because of the intricacies involved making in-vitro neuronal networks that accurately mimic in vivo cellular architecture. The cerebral cortex is patterned into six layers with each neuron forming connections with other neurons throughout the layers[12]. While different research groups have different methodologies for patterning, they are all based on standing waves. Standing ultrasound waves generate areas of high and low pressure at antinodes and nodes respectively. The cells can be patterned at the nodes and their spacing can be adjusted by modulating the ultrasound wave frequency.

Bouyer et al utilized the principles of acoustic forcing, via standing waves, to create brain-like 3D constructs without using a printer[13]. This paper demonstrated how acoustic forcing can be used to "levitate" cells into six layers to accurately recapitulate the 3D microenvironment of the in vivo cerebral cortex. An overview of this methodology is shown in Figure 3[13]. However, this model lacked connectivity between each layer.

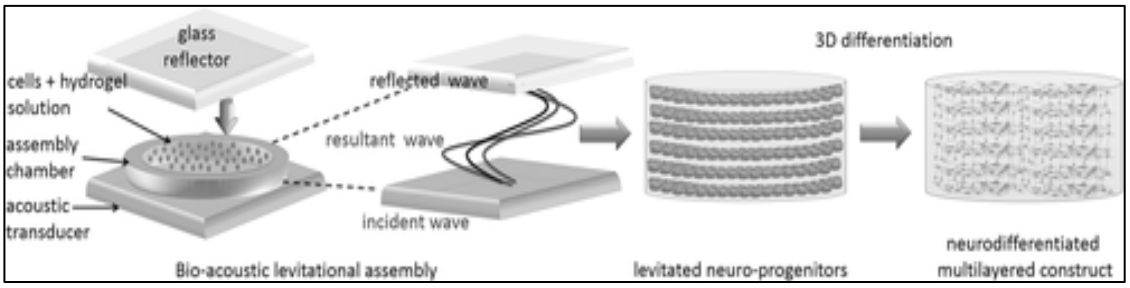

Figure 3. Experimental set up by Bouyer et al utilizing standing acoustic waves at different levels to create a multilayered 3D construct of neural progenitor cells[13].

Cohen et al further showed that patterning of neurons could also direct the directionality of neurite growth[14]. This group utilized a radial transducer which patterned the seeded neural cells into concentric rings. Each ring of cells had branching neurites with neighboring rings. The acoustic forcing imparted on these cells did not reduce their viability. Utilizing this patterning methodology can prove to be invaluable in developing tissue systems that accurately model complex systems such as the cerebral cortex[15,16].

Wang et al, following the work of both Bouyer and Cohen, developed neural constructs that could present a simplified version of the six-layer cerebral cortex tissue with intra and inter layer connectivity[12]. This methodology utilized a radial transducer to produce concentric rings of neurons with human-mimetic spacing of 400-μm. Wang showed that the patterning could be done with neural stem cells as they differentiate or with already mature stem cell derived neurons. The model with differentiating neural stem cells could be used as a model for studying neurodevelopmental disorders. The model with mature neurons showed strong intra and inter connectivity and increased activity compared to the differentiating neural stem cell model. Wang et al demonstrated the potential use case of studying neurodegenerative disorders by inducing the above models with Alzheimer's disease like features[12]. HSV-1 induction is a common method used in creating Alzheimer based models. Key features of this model include increase production of amyloid plaque protein and increased neuronal death. They found that the HSV-1 treated patterned tissue expressed a significant increase in amyloid protein production and decrease in neuronal viability compared to untreated tissues[12].

2.1.3 Cell Differentiation

In addition to its use in improving bioprinting outcomes, acoustic forcing has also been used in studies to accelerate or enhance stem cell differentiation. Stem cell differentiation is one of the fundamental building blocks of tissue engineering. This is due to its ability to facilitate personal medicine treatment options, reduce the need for donor tissue sources, and its innate regenerative capabilities.

Several studies have been conducted with a focus on identifying whether, and if so, how ultrasound forcing can be used to induce or improve stem cell differentiation. Sun et al found that exposing human embryonic stem cells in a neural induction medium to acoustic accelerated the differentiation of these cells into mature neurons[17]. This group stimulated the hESCs in a neural differentiation media with a range of RF amplitudes (24V, 31V, 34V) for a period of 12 days and then cultured them for an additional 10 days without stimulation. They were then analyzed via qPCR and staining for neural progenitor markers and mature neuronal markers. As shown in Figure 4a, the stimulated groups reported significantly less or similar levels of expression of progenitor neural genes, such as PAX6, SOX2, SOX10, and Nkx2-1[17]. Histological staining for the mature neuron marker Tuj1 and progenitor marker SOX2 found that the Tuj1:DAPI staining ratio was significantly higher and the SOX2:DAPI staining ratio significantly lower in the stimulated groups compared to the control groups as shown in Figure 4b[17]. This indicates that the hESCs were differentiating at a faster rate when exposed to acoustic waves because they expressed a smaller amount of progenitor associated genes and displayed a larger amount of

mature neuronal associated markers[17]. Potential reasons for this increase in speed of cell differentiation is that the mechano-sensitive elements of a cell, such as the ECM-integrin complex, play a significant role in regulating the neuronal development of stem cells. Thus, the physical disturbance induced by the acoustic wave application may impact this complex in such a way that accelerates neuronal development[18].

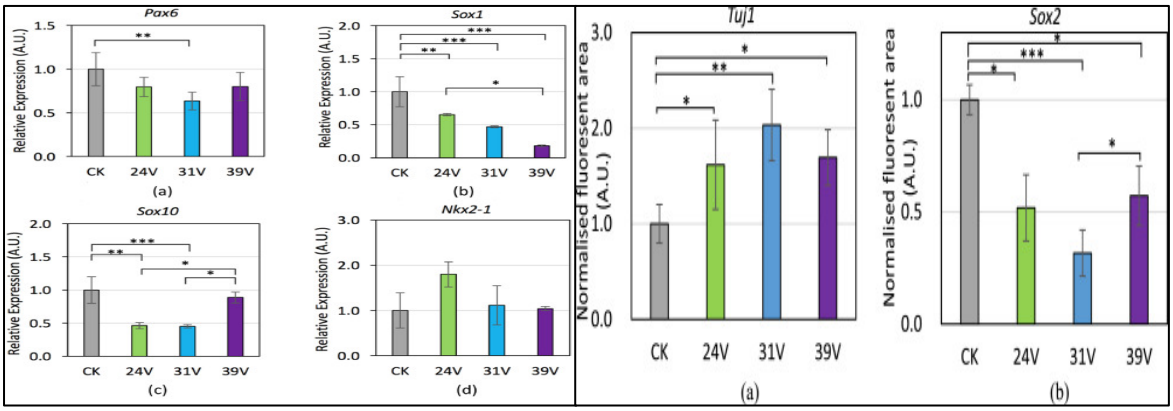

Figure 4. Fig 4a(left) qPCR reporting expression of neural progenitor data normalized to the control group expression. Figure 4b(right). Fluorescence of Tuj1 and SOX2 markers normalized over DAPI fluorescence[17].

To summarize this chapter, acoustic forcing has been used in applications to improve tissue engineering methods. This includes improving printing and patterning results to yield more accurate organ models and cell differentiation to improve cell sourcing for producing such models.

2.2 Lab on Chip Technology

Lab on a Chip (LOC) systems are a heavily researched technology whose target goal is to take a given sample, isolate the targeted analyte within the sample, and detect the targeted analyte on a miniaturized platform away from the lab. LOCs increase the availability of potential testing because of its portability and cost savings. These cost savings arise because of the lack of a need for a lab and the associated

costs with shipping samples to/from the lab and operating costs for the lab. LOCs are popularly used as diagnostic tools ranging from environmental to medical case uses. With the focus of this thesis on acoustic forcing in bioengineering, LOCs is discussed in its medical case uses. Improvements to create better LOCs have opened the door for utilization of acoustic forcing.

LOC diagnostic technologies are typically split into three parts: sample collection, analyte isolation, and analyte detection[19]. Proper analyte isolation by the LOC system is critical to its success because if the analyte is not able to be properly isolated, its proper detection is impaired. This skews the detection which invalidates the entire purpose of the LOC.

Blood is a very common sample used for analysis in LOCs. Blood is made up of two parts: 55% plasma and 45% blood cells. The plasma portion is particularly popular for use in diagnosis and prognosis of disease specific antigens because it is likely to contain markers, such as antibodies or DNA/RNA fragments, that are indicative of the disease[20]. Standard methods of plasma isolation involve the use of centrifugation, but this is very costly and time consuming. Thus, acoustic forcing principles streamline this isolation process in LOCs.

Liu et al utilized acoustic forcing to induce microstreaming to create a device that could separate plasma from the cells in blood[21]. Ultrasound waves, when applied to air bubbles in media, generate eddy-like closed-streamline vortex[22]. The generated device had pockets attached to the main channel that contained air bubbles. Ultrasound waves, emitted by a piezo plate attached to the device, are directed onto the air bubbles as the blood flows through the channel. The microscale red and white

blood cells are caught in the generated streaming vortex while the nanoscale plasma constituents can continue flowing. This process is repeated multiple times throughout the channel, resulting in the cell content within the fluid decreases as the blood continues down the channel. Figure 5 shows a diagram of what happens when the streaming vortices are created. The right section of the figure shows how the blood plasma is filtered as it continues down the channel from a to e while the cells are captured in the vortexes by the air bubble/liquid interface. The number of cells and amount of plasma were calculated at the collection port. 31.8% of the initial plasma volume remained with 99% of cells removed[21]. The plasma extracted by a standard centrifuge is about 55% of the initial blood volume showing that this methodology does show promise[21].

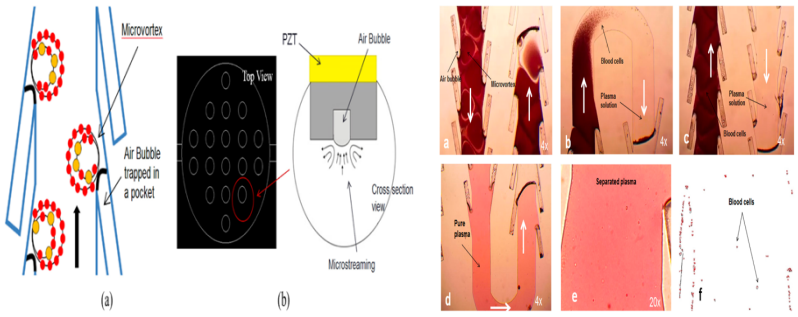

Figure 5. Diagram showing how streaming vortices trap red blood cells which filters them out from the plasma in the device created by Liu et al[21]..

This acoustic forcing principle can also be applied to isolation of cancer cells from blood. Circulating tumor cells (CTCs) are a critical part of cancer biology research because their presence is indicative of cancer prognosis and metastasis. CTC monitored presence can also be referenced when determining the efficacy of a treatment method. However, isolating CTCs effectively proves to be a large issue. CTC isolation is divided into two types: antibody-dependent and antibody

independent. The antibody dependent methodology uses fluorescent antibody markers that bind to the CTC to mark them. However, the flaws of this method are that this only works if the CTC markers are known and is time and cost expensive[23].

Antibody-independent isolation leverages the fact that CTCs innately differ mechanically from blood cells. Thus cells of varying sizes and mechanical properties can be separated from each other[24]. Using these principles, Li et al fabricated a device that utilized angled surface standing acoustic waves (SSAWs) to isolate CTCs from a mixed cell suspension[23]. As shown in Figure 6, the sample fluid containing the cells are injected into a channel. Interdigitated transducers (IDTs) are placed on either side of the channel at an angle and generate angled SSAWs. These SSAWS force the CTCs and other cells into different streams that end up in separate channels. Li et al demonstrated that this device could successfully separate various types of CTC lines from the white blood cells (WBCs) they were mixed with including UACC903M, LNCaP, MCF-7, and HeLa cell lines[23]. Various CTC:WBC ratios were also tested. CTC recovery rates for each tested trial exceeded 80%[23].

LOC devices are based on an interplay between acoustic radiation force and acoustic streaming. Acoustic streaming occurs when the bulk flow of radiation force acting upon a fluid generates patterns of flow within a fluid medium. Therefore, the generation of these flow patterns is called acoustic streaming[25]. The radiation force acts on individual particles/cells while the streaming effect carries the particles/cells within stream patterns. The interplay between radiation force and drag force from streaming used for separating particles is based on particle size and density[26].

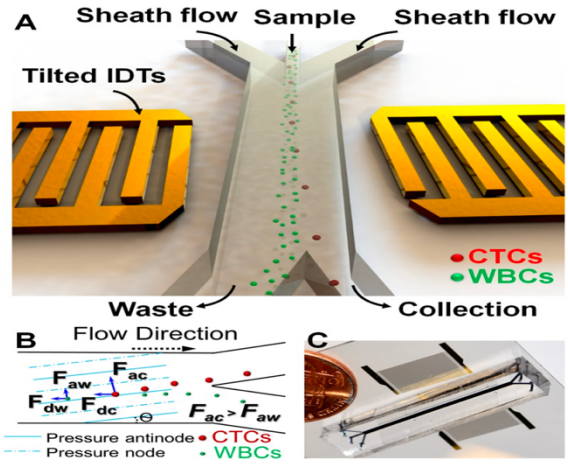

Figure 6. Standing acoustic waves, produced by IDTs, are used to separate CTCs from WBCs based off their different densities in the device created by Li et al[21].

2.3 Drug Delivery

Acoustic forcing has also been investigated in relation to improving drug delivery methodology. Drug delivery is a very complex process that is constantly being refined in terms of proper localization and duration to improve efficacy and reduce systemic toxicity[27]. One of the most widely used ultrasound-based drug delivery methods is microbubbles.

Microbubbles are spherical objects with a gas core and a solid shell. Such a shell is typically made of a polymer, lipid, or protein. Such microbubbles are ideally non-toxic, intravenously injectable, and have a diameter less than 8 μm to be able to pass through capillary beds when in circulation[28]. The microbubbles are typically used as contrast agents because of how its gaseous core's acoustic impedance differs from blood's impedance[4]. Additionally, the application of the ultrasound on the microbubbles cause the bubble to expand and contract as the wave transverses the bubble - a process known as cavitation[29]. Applying low acoustic power waves causes the bubbles to vibrate which opens holes in the capillaries to improve drug delivery

efficacy. By increasing the power, the bubbles vibrate with increasing intensity until they rupture. This ability, known as sonoporation, to permeate vasculature is useful in situations where natural biological barriers such as blood brain barrier (BBB) or modified barriers such as in tumors are present[29].

The BBB is a part of the vascular system in the brain that contains endothelial cells connected together by tight junctions to insulate itself from the rest of the brain[30]. Its limited permeability ensures that toxic substances found in the blood do not leak into brain tissue. However, this limited permeability also limits brain-targeted drug delivery because the drugs in circulation are not able to pass into the targeted brain tissue. Thus, efficacy in treatment of brain-related diseases has been limited[30]. Focused ultrasound stimulation (FUS) on microbubbles has been demonstrated by several research groups to transiently open the BBB to allow for drugs to enter[31–33].

Tumor vasculature is a very complicated system that does not conform to the typical vessel morphology[34]. The use of ultrasound and microbubbles leverages this difference in tumor vasculature to disrupt the vessels. Damaging these vessels would in theory then reduced perfusion to the tumor and increase permeability to drug treatments. Goertz et al conducted a study in which ultrasound stimulation of microbubbles was carried out on PC3 tumors implanted in mice with and without Docetaxel, a common chemotherapy drug . Figure 7a shows that the combination of ultrasound with microbubbles and Docetaxel led to the greatest reduction in tumor volume compared to each individually and Figure 7b shows how the combination also reduced the amount of perfusion in the treatment[35].

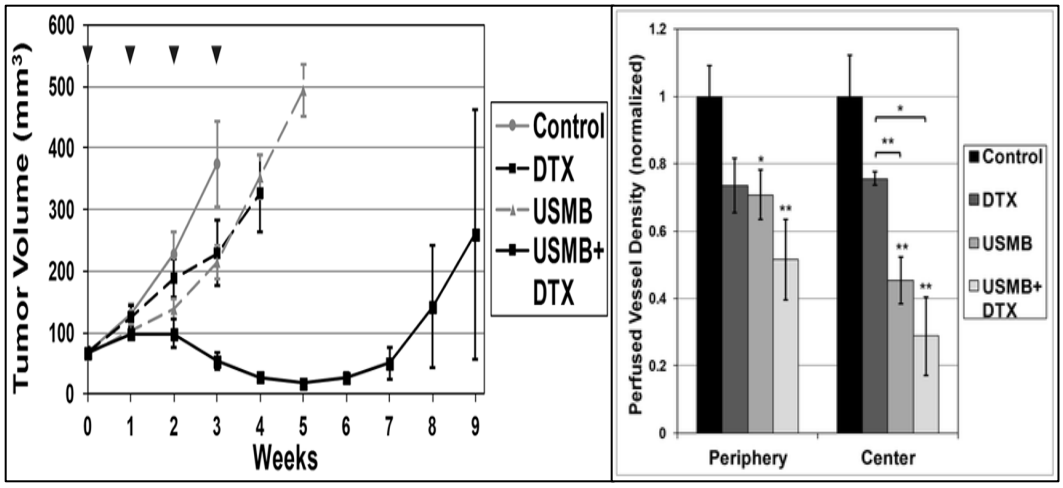

Figure 7a.(left) Chart depicting how tumor size is impacted over time by different treatment options including: Docetaxel, ultrasound stimulated microbubbles, and Docetaxel with ultrasound stimulated microbubbles. A combination of Docetaxel and microbubbles reduced the tumor volume the greatest. Figure 6b. (right) Bar chart depicting the vessel density within tumors in different treatment groups. The synergetic use of microbubbles and Docetaxel reduces tumor vessel formation the greatest. This data is based off the work from Goertz et al[35].

The components of the microbubbles, including the type of gas in the core of the bubble, and the shell material have been at the forefront of research in ultrasound-microbubble drug delivery. Microbubble technologies have also expanded to exceed usage of just being co-administered with a drug product[36]. Such technologies focus on loading drugs and or therapeutics into the center or onto the surface of the microbubble rather than having free drug products injected[36]. The reasoning for this is that it increases bioavailability and limits the amount of healthy tissue adversely impacted by said drug/therapeutic[37]. The potential drawbacks, however, are that the amount of space within a single microbubble is limited for the drug/therapeutic and the drug/therapeutic biological activity may be impaired when in the microbubble[36,38].

To summarize, efficient drug delivery is a complex process that is often blocked by natural barriers. Microbubbles are a mechanism that is heavily

investigated to bypass said barriers. The application of acoustic forcing on microbubbles shows great promise in enhancing drug delivery outcomes.

Chapter 3: Acoustic Forcing Mechanics

This chapter discusses the theory behind acoustic forcing and its applications. First, ultrasound fundamentals are discussed. This includes surface vs bulk acoustic waves, low vs high intensity, standing vs travelling waves, and pulsed vs continuous waves. The second part of the chapter will discuss the principles behind the bioeffects of ultrasound stimulation at the cellular level.

3.1 Fundamentals of Acoustic Forcing

Ultrasound, by definition, is sound waves at ultrasonic frequencies. These frequencies are greater than 20 kilohertz. Ultrasound technology is fundamentally based on the piezoelectric effect. This effect is essentially the conversion between electrical and mechanical energy. In the specific context of acoustic forcing, electrical energy is sent to the chosen transducer which in turns converts this energy into mechanical energy to cause vibrations which produces the “acoustic” force. Common piezo materials can be classified into different categories including: single crystalline material such as quartz, piezoceramics (lead zirconate titanate), piezoelectric semiconductors (zinc oxide), polymers (polyvinylidene fluoride), and glass ceramics (Li2Si2O5)[39].

The use of acoustic forcing in various applications in biological environment can be split into thermal and non-thermal effects. The thermal effect of ultrasound, at high intensities, results from the absorption of the energy from acoustic waves by an

object. The given medium absorbs this energy and experiences an increase in temperature[40]. This is the mechanism used in ultrasound-based ablation. The non-thermal ultrasound bioeffects include cavitation, radiation force, and streaming force. Acoustic waves generated by piezoelectric plates are generally separated into Surface Acoustic Wave(SAW) and Bulk Acoustic Wave (BAW)[41]. SAWs propagate acoustic waves along the surface of the chosen interface while BAWs transmit acoustic waves through the bulk of a material.

3.1.1 Surface Acoustic Waves vs Bulk Acoustic Waves

SAWs typically use interdigital transducers (IDT) plated on piezoelectric substrates to create the acoustic waves along a substrate's surface[42]. These IDTs are essentially just metal film deposits on the substrate. A voltage source is connected to the metal deposits which then generates a wave along the substrate towards the other end of the substrate which also usually has an IDT plated on. The IDT at the other side of the substrate can then pick up the incoming acoustic wave and generate a voltage across itself. Alterations along the surface of the substrate can change the flow of the waves from one IDT to the other IDT which in turn could impact the voltage measured by the receiving IDT. This makes SAWs a popular choice for biologic/chemical testing because the testing marker would impact the traveling acoustic wave and thus the measured voltage along the receiving IDT. Figure 8 shows a general schematic of how IDTs are used in detection devices[43]. A "sensitive" zone would be placed in between the two transducers which would pick up the desired diagnostic molecule and impair the acoustic wave accordingly.

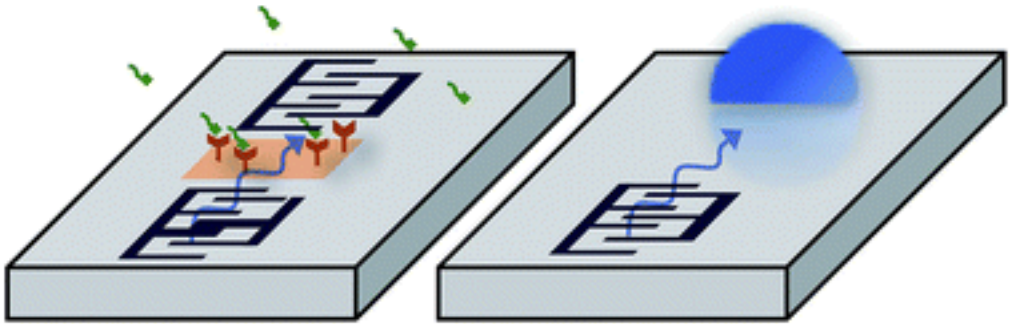

Figure 8. Diagram representation depicting how SAWs can be used as a sensor for biologic/chemical testing[43].

When both IDTs have voltages applied on them, they both produce waves causing the formation of standing waves. SSAWs are particularly useful for patterning objects at the micron-scale. As shown in Figure 9**,** the standing waves create pressure nodes where the net pressure is 0[44]. The particles typically are forced into these pressure nodes. Wave parameters, such as frequency and amplitude, can impact how far apart the targeted particles are spaced and the amount of time it takes for them to be spaced[44].

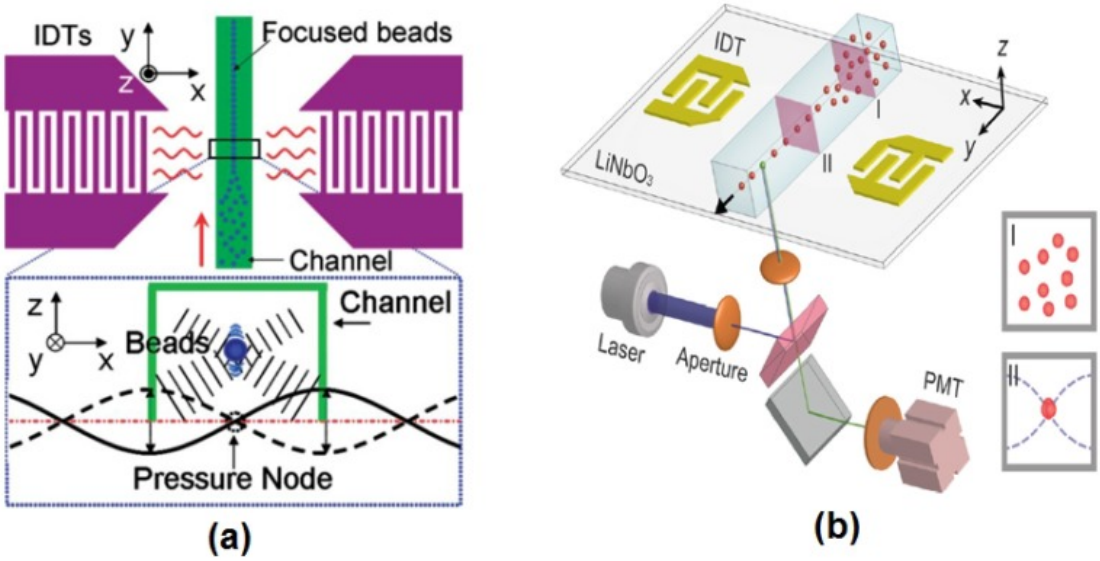

Figure 9. Figurative representation of how standing SAWs are used in IDTs to pattern micro-sized particles[44].

There are several different types of SAWs including Rayleigh waves, Lamb waves, and shear-horizontal waves. Rayleigh waves are widely used in microfluidic device fabrication because of their ability to induce acoustic streaming in a liquid. The resonance frequency of an IDT is mainly dependent on its geometric design and material. Its resonance operating frequency (f_o) is given by the following equation with v_s being the acoustic velocity of the substrate and p is the periodicity of the IDT which is the wavelength of the propagating SAW at the resonance frequency[45].

$$f_o = \frac{v_s}{p}$$

BAWs are acoustic waves that propagate across the bulk of a medium. BAWs can be categorized into longitudinal and transverse waves. The longitudinal waves move particles parallel to the waves while transverse waves move particles perpendicular to the wave. The resonance frequency of BAW is given by the following equation[46].

$$f_r = \frac{v_L}{2h}$$

Its resonance frequency (f_r) is given by the following equation with v_L being the velocity of longitudinal waves in the direction of plate thickness and h is the thickness of the piezo plate[46]. Figure 10 shows how BAW propagate[47].

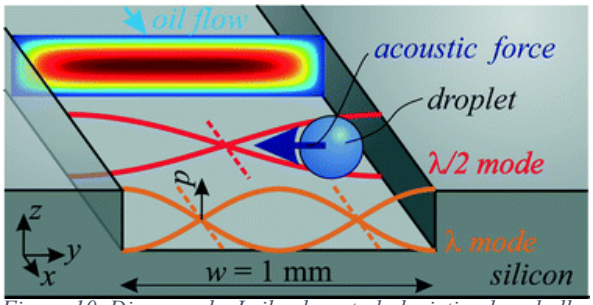

Figure 10. Diagram, by Leibacher et al, depicting how bulk acoustic waves propagate and can pattern particles[47].

BAW modality is used in a popular use of ultrasound - imaging. In ultrasound imaging, the transducer emits acoustic waves which travel through the medium body. The waves hit an object in the body, such as bone, and reflect onto the transducer. The transducer picks up these returning acoustic waves to generate an image. Each tissue type in the body has its own unique composition. This difference in composition of each tissue allows each to have its own acoustic impedance. As a result, the waves thus return at different speeds, thus allowing the unique identification of each individual part of the body. BAW waves operate better at lower frequencies and longer wavelengths than SAW waves, allowing them to be used for handling larger particles[47].

3.1.2 Low Intensity vs High Intensity

While acoustic waves can be classified according to the way they propagate, Bulk vs Surface Acoustic Wave, they can also be categorized into low-intensity vs high-intensity waves. A wave's intensity is indicative of the amount of energy it carries. High-intensity ultrasound waves have intensities of greater than 100 W/cm^2 while low-intensity ultrasound waves have intensities in the 0.125 to 3 W/cm^2 [48]. High-intensity waves convert into thermal energy and are typically used to ablate tissue while low-intensity waves are used for inducing mechanical stimulus at the cellular level for nondestructive goals such as inducing regenerative effects or facilitating drug delivery[48]. Imaging ultrasound typically uses low intensities of around 0.1 W/cm^2 [49].

3.1.3 Standing vs Traveling Waves

Ultrasound waves can be classified as standing and traveling waves. Standing waves are formed when two waves of the same frequency and amplitude travel in opposite directions intersect each other. This can be done with two piezoelectric transducers placed opposite of each other and driven at the same frequency and same voltage or with one transducer and a reflecting material. The standing waves stay stationary in the given medium with areas of high pressure at the anti-nodes and low pressures at the nodes. Standing waves can be generated using one transducer and one reflector, or two transducers placed opposite each other. Standing waves are typically used for patterning particles such as cells[50].

Traveling waves, on the other hand, propagate through a medium. This type of wave is generated from a single transducer and is not constrained by any reflector or additional transducer. The traveling wave will reflect off different objects differently. The reflections of acoustic waves generates the images in imaging ultrasound[28].

3.1.4 Pulsed vs Continuous Wave

Ultrasound waves can additionally be separated into continuous or pulsed waves. Continuous waves are emitted for an uninterrupted period until the energy of the wave dissipates. Pulsed waves are waves emitted in periodic bursts with intermissions of no emission in between them. Each type of wave has its own set of use cases and benefits in applications. Continuous waves are often used at high intensities to ablate tissue while pulsed waves are used at low intensities to induce sub-cell changes[51]. There is discrepancy between studies about whether continuous or pulsed waves at low intensities are better for inducing neuromodulation effects[52–54].

3.2 Physical Mechanisms of Acoustic Forcing and Cells

There are generally three main phenomena mentioned when discussing the mechanisms by which acoustic forcing impacts cells. These include inducing temperature rise, bubble formation cavitation, and acoustic radiation force[55]. Temperature increases associated with ultrasound applications are due to absorption. This phenomenon results in the conversion of mechanical energy, from ultrasound waves, into heat[56]. Temperature increases are significant at high intensities.

Cavitation effects of ultrasound work by the formation of new bubbles or expansion of already existing bubbles in a liquid. The oscillation of the acoustic waves causes the bubbles to increase and decrease in size. Cavitation can be either stable or transient. In stable cavitation, these bubbles then increase in size until they explode. In stable cavitation, the bubbles experience periodic expression/compression over a period of many cycles. In transient cavitation, the bubbles expand and explode in a short number of cycles[57]. Endogenous microbubbles formation occurs via pockets of gas found within the body. These microbubbles have a cavitation threshold that is proportional to the square root of the ultrasound frequency. Thus, endogenous microbubbles formation typically occurs at lower frequencies (10-100s kHz) because a smaller intensity threshold is required compared to higher frequencies[38].

Acoustic radiation force (ARF) develops as a result of energy transfer from a ultrasound field to a specific object via a propagating media[40]. ARF acting on a compressible spherical object within a standing wave can be approximated by the follow equations[26]:

$$\boldsymbol{F_R} = -\left(\frac{\pi p_o^2 V_p \beta_f}{2\lambda}\right)\phi\left(\beta,\rho\right)\sin\left(\frac{4\pi \boldsymbol{x}}{\lambda}\right)$$

$$\phi\left(\beta,\rho\right) = \frac{5\rho_p - \rho_f}{2\rho_p + \rho_f} - \frac{\beta_p}{\beta_f}$$

The p_o and V_p represent the acoustic pressure and volume of the particle. β_f, ρ_f, β_p, and ρ_p are the compressibility and density of the fluid and particle. Φ is the acoustic contrast factor, λ is the acoustic wavelength, and x is the distance from a pressure node[26]. This typically can be used to move objects, as in cell patterning, or, for the purpose of this thesis, stimulate mechanosensitive proteins in the cell membrane.

Yoo et al conducted a study that investigated all three of the above-mentioned ultrasound cellular effects. The paper found that focused ultrasound excite murine cortical neurons through mechanical stimulation of calcium-selective mechanosensitive ion channels[55]. This finding will be discussed in greater depth in the next chapter.

Chapter 4: Acoustic Forcing in the Context of Living Neural Networks

This chapter details the work I have done for this thesis. The chapter will begin with going over background and prior research about acoustic forcing in neural network-based studies. After that, my methodology from experimental set up through

analysis is described. A discussion of results and conclusion, including limitations and future works, will end the chapter.

4.1 Background

Neural network development is an extremely complex and vital part of organismal development because it enables an organism to process external stimuli and operate accordingly. The sharp increase in neurological disorders, now affecting around 15% of the world's population, has only further highlighted the need to understand how the neurological system works[4]. This can be done through the production of biomimetic neuronal network structures and understanding how such networks work in both normal and diseased conditions. Developing these models and understanding the mechanistic functions in normal and diseased conditions can improve treatment and therapeutic methods to better treat neurological disorders.

4.1.1 Acoustic Forcing-Mediated Cell Patterning

As mentioned earlier in Chapter 2, acoustic forcing has been used, via cell patterning/printing and differentiation, to successfully produce biomimetic neural structures such as cerebral cortical tissue. As previously mentioned in Chapter 3, standing acoustic waves occur when two waves are traveling in opposite directions at equal amplitudes and frequencies. This can be done with either two transducers placed on opposite sides of each other or with one transducer and a reflecting plate. The pressure from the waves pushes cells into the regions of low pressure: nodes. Several studies have already demonstrated the ability to use standing acoustic waves to develop neuronal constructs and direct neurite growth[12–14]. Wang et al fabricated

six-layer concentric neuronal rings that resembled cerebral cortices in both number of neuron layers and spacing between layers via standing acoustic waves. Figure 11 shows how these neuronal structures physically looked. Such structures can be instrumental in studies focusing on understanding how neurodegenerative diseases function and their potential treatments[12]. Another important use of acoustic forcing of neural engineering is neuromodulation.

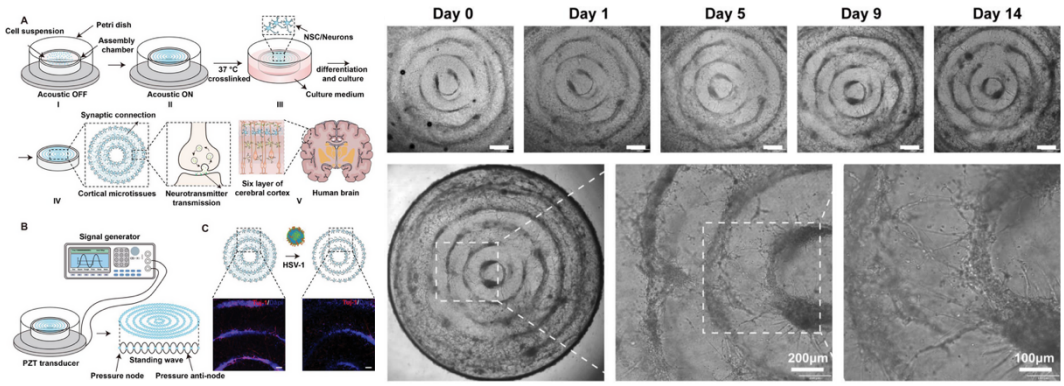

Figure 11. On the left is a figurative representation showing how Wang et al patterned cerebral cortices-like constructs. On the right are microscopy images showing how the constructs look over the course of 14 days[12].

4.1.2 Acoustic Forcing-Mediated Neuromodulation

Neuromodulation, the alteration of nerve activity through stimulus delivery, is a popular research area in treatment development for treating neurological related diseases. The stimulus either stimulates or inhibit neuronal signaling within the nervous system. There are various types of stimuli used in neuromodulation including magnetic, electrical, optogenetic, thermal, chemical, and acoustic[58]. Acoustic or ultrasound neuromodulation is an increasingly popular subsection of neuromodulation. Its non-invasiveness and high-spatial resolution make it a particularly popular branch with deep brain stimulation[59]. While numerous trial studies have been conducted to how different ultrasound parameters can modulate

neuronal activity, there is no clear understanding behind the mechanism of inducing excitation vs inhibition yet[60]. The only currently FDA approved use for trans-cranial ultrasound is for tremor ablation in patients afflicted with Parkinson's disease[60]. Thus, understanding mechanism which describes how ultrasound waves affects neuronal activity is critical in the development of ultrasound-based treatment for neurological related disorders[61].

Standing acoustic waves are an important part of ultrasound-based neuromodulation. This is specifically true in trans-cranial based neuromodulation in both single and double transducer use. The concave design of the transducer ensures that there is a focal point where the waves are concentrated the greatest. When utilizing a single transducer, the ultrasound waves applied to the brain may interact with the distal part of the skull and reflect to generate standing waves[62]. This generates unwanted pressure gradients within the skull whose effects may have potential implications in causing hemorrhages[63]. Patterned interference radiation force (PIRF) is a newer proposed transcranial neuromodulation method that utilizes two transducers to concentrate its waves on a specific part of the brain to induce an action[64]. The interaction of waves from both transducers forms a standing wave that can offer higher spatial resolution and greater power efficiency compared to a single transducer[64,65]. Figure 12 shows how focused trans-cranial ultrasound works with one vs two transducers[64]. The impact of standing waves on neuronal networks like the brain, whether intended or not, are not entirely clear.

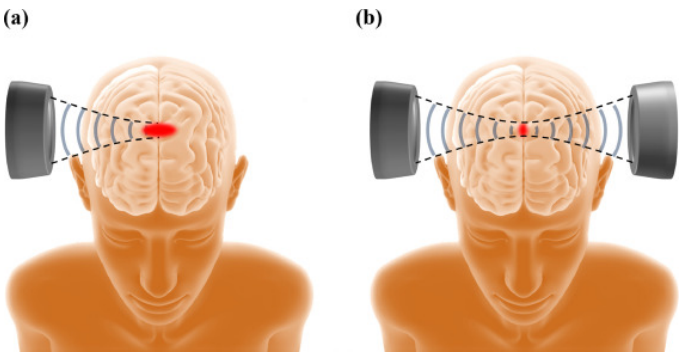

Figure 12. Figurative representation of how trans-cranial focused ultrasound works with one (left) and two (right) transducers[64].

As mentioned in the previous chapter, ultrasound application can produce a variety of effects on cells including cavitation, heating, and mechanical deformation. Yoo et al investigated which of these effects are involved in neuromodulating cortical neurons. They found that ultrasound excites primary murine cortical neurons mainly through calcium-selective mechanosensitive ion channels[55]. Yoo et al additionally identified the TRPP1/2, TRPC1, and Piezo1 mechanosensitive ion channels involved in the neuron's response to ultrasound stimulation[55]. Their study also found that other ultrasound bioeffects, such as cavitation and temperature change, do not significantly contribute to ultrasound-stimulated neuronal activity. The research group ran these studies using ultrasound stimulation via traveling continuous waves from a piezo plate at 300 kHz and a plate at 670 kHz shown in Figure 13a. Figure 13b shows the increase in neural activity, measured via calcium entry, with increased wave

intensities and durations.

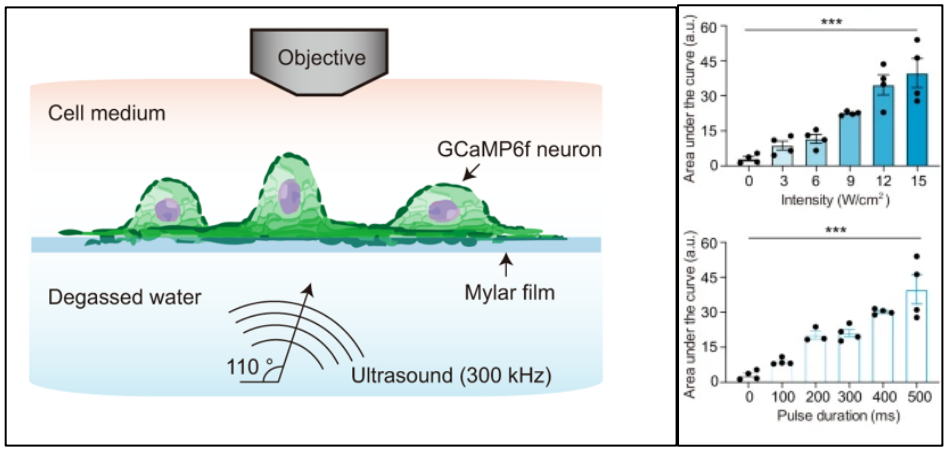

Figure 13. 13a (Left) Schematic showing how experimental set up of ultrasound forcing on cortical neurons. Figure 13b (Top right) Quantification of calcium neural response as a function of ultrasound intensity and wave duration (bottom right)[55].

However, this study did not investigate the potential impact of static pressure gradients caused by standing waves, which could be present in vivo or in vitro preparations, and is noted to potentially give more information about ultrasound's impact on neurons. Additionally, the study only focused on ultrasound impact on individual cortical neurons. This is not representative of understanding ultrasound stimulation of neurons in vivo because such neurons would be found in connected networks rather than individual cells. The ultrasound waves used in this study were also only traveling waves which would not be true for in vivo applications. In-vivo ultrasound applications, particularly in trans-cranial focused ultrasound, can cause standing wave formation[5].

A study was conducted to investigate whether bulk acoustic standing waves had any impact on cellular viability and metabolic activity. Diaz et al specifically investigated whether and how the cell viability and metabolism for human dermal fibroblasts (HDF) and cervical cancer cell line (HeLa) were effected[66]. Variations

were made in incubation temperature, 20 vs 34 degrees centigrade, exposure time, of 5, 10 and 15 minutes, and voltage, 4-10 Vpp. A frequency of 6.74 MHz was kept constant. The study found that both cell types had unique preferences for incubation temperature, ultrasound voltage exposure, and exposure duration[66]. Cell viability was better at 20 degrees Centigrade but suffered from increased cell metabolism which can be an indication of cell toxicity[66]. Diaz et al found that refinement of the protocol for acoustic forcing, regarding temperature, exposure time, and voltage exposure, needs to be investigated thoroughly to clearly elucidate their impact on cells.

Thus, to summarize, neuromodulation via ultrasound is a popularly proposed treatment method to correct impaired neural activity. Standing acoustic waves has been successfully used in cell patterning applications. However, its potential impact on wide-scale neural network activity is not well-understudied. This is specifically important in transcranial focused ultrasound applications because of the prevalence of standing waves in the method. Menzer et al utilized standing acoustic waves on ex vivo salamander retinas and found standing waves did increase neuronal activity but was not necessary for activity[67].

The basis of my work is to investigate whether acoustic forcing, via standing acoustic waves and the pressure gradients, creates changes in neural network activity. Based on previous studies, which have shown the mechanosensitive ion channels to be the main ultrasound stimulation target, I hypothesize that the application of the acoustic standing waves should increase neuronal activity within a network[55,68,69]. The independent variables that will be investigated are network age and the acoustic forcing intensity used and it the dependent variable is network activity. The main

objectives of this study include fabricating a device that can propagate standing waves onto a plated neural network and reporting the network activity in its response to standing waves.

4.2 Methodology

4.2.1 Device Fabrication

To produce acoustic standing waves, I fabricated a device that could be placed in the petri dish of cultured neurons and emit standing acoustic waves. This was done by first modeling the device design in AutoCAD Fusion 360 and then printing it in Formlabs Clear Resin with a Formlabs V3 printer at Terrapin Works at the University of Maryland. This specific resin material was previously tested for cytotoxicity as a possible bioreactor material. Among the available resins at Terrapin Works, including black, clear, flexible, and high-temperature resin, Kreb et al found that that the clear resin reduced cell viability the least compared to other resins[70]. It also should be noted that the work done by Kreb et al incubated the cells with the resin overnight compared to the brief exposure the device would have with the cells in the experiments in this thesis. The device, whose dimensions can be seen in Figure 12, was designed to be able to rest on the outskirts of a 35 mm glass coverslip petri dish. The piezo plates slots are lowered into the coverslip region, where the hNPCs are plated 0.75 mm below the rest of the dish, by 0.70 mm. This is done to ensure more of the acoustic waves from the piezo plates can interact with the cells without the device crushing the cells.

Lead zirconate titanate rectangular plates (PZT-850) were purchased from American Piezo Ceramics. The plates measured 15 mm by 10 mm by 1 mm. The resonance frequency, calculated by American Piezo Ceramics based on the plate's thickness and material type, is 2.04 MHz. While trans-cranial focused ultrasound is typically done to stimulate neural activity at frequencies below 1 MHz, newer studies have found higher frequencies, up to 5 MHz, still provide neurostimulation while also providing greater spatial resolution[71]. The PZT plates were placed, with Loctite epoxy adhesive into the slots in the 3D printed part of the device and set to adhere for 24 hours. The slots were created to ensure no direct contact between cells and Wires were then soldered onto each piezo plate such that the function generator connected with pair of wires to each plate. For acoustic forcing, the function generator was set to produce continuous sinusoidal waves at its resonance frequency of 2.04 MHz. The piezo plate's intensity is calculated via the equation I = P/A with P the power and A is the surface area of the plate. The power, calculated as the product of V_{rms} and its current, at 10 Vpp (peak to peak voltage) and resonance was calculated as 2.86 watts. The surface area of 1.5 cm^2 yields an intensity of 1.9 W/cm^2. The piezo plate functionality was tested by connecting the function generator with the wires and turning the function generator on with sinusoidal waves at an audible frequency (~12 kHz). Figure 14 shows the device schematic and Figure 15 shows what the final

device looks like.

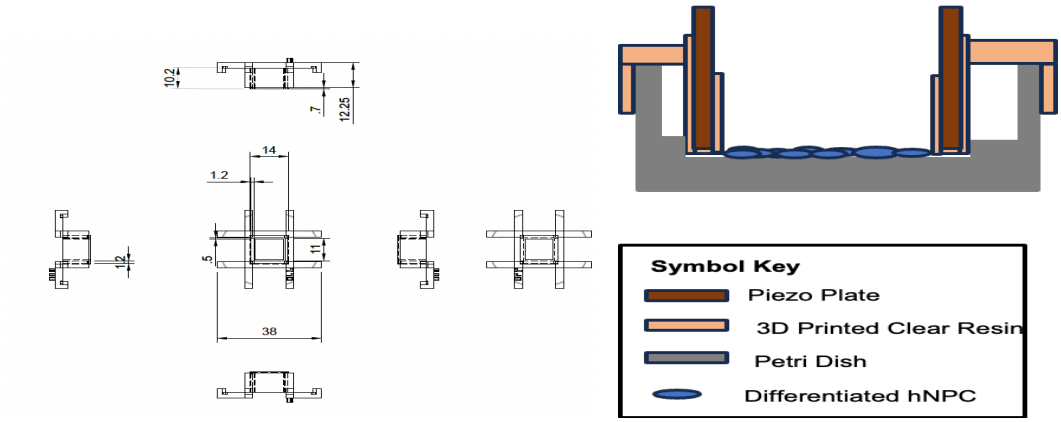

Figure 14. Schematic drawing of device dimensions (left) and figurative representation of how deice fits in petri dish (right).

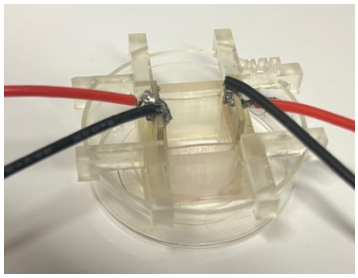

Figure 15. Picture of the constructed device in culture petri dish.

4.2.2 Imaging

Neuron activity was tracked via calcium imaging[72,73]. Calcium imaging is a popular imaging modality for tracking neuronal activity because of its role in depolarization of the cell membrane as it reaches its action potential[72]. When a neuron reaches action potential, indicating a firing of the neuron, there is a large influx of calcium into the active neuron. Calbryte-590 AM (AAT Bioquest) is a fluorescent dye that was used to track calcium activity. The Calbryte was added to a culture dish containing the neural network and set to incubate for 45-60 minutes before the media

was removed and replaced with fresh media. The plate is then set up in the incubator of the in-lab multiscale microscope for imaging.

Imaging for both the microbead patterning and cell experiments were done using an in-lab built multiscale microscope whose set up is depicted in Figure 16. This microscope contains fluorescence widefield and confocal microscopy capabilities. For this project, focusing on imaging neural network activity, the fluorescence wide field's simplicity and ability to capture a large 2D field of view is sufficient. The confocal scope could be used in future experiments to focus on individual cell activity. The microscope also contains an on-stage incubator to ensure cells remain viable during imaging.

4.2.3 Cell Culturing

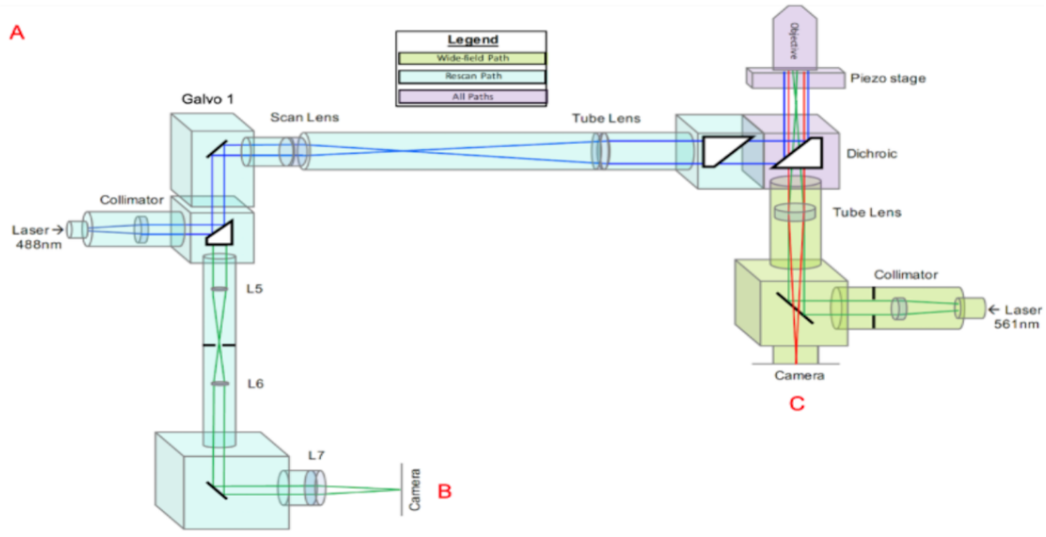

Figure 16. Figurative representation of the in-lab built multiscale microscope used for imaging.

The ReNcell VM (Sigma Aldrich) immortalized human neural progenitor cell line was used for these experiments. These ReN cells can differentiate into neurons

and glial cells which makes them a more accurate biomimetic model to the brain. The undifferentiated cells are plated at a density of 3 x 10^5 on a laminin coated petri dish, per manufacturing specifications, and then allowed to differentiate. Laminin coating was used to enhance cell attachment to enhance network formation and maintain cell viability. The ReN cells typically take 14 days to fully differentiate but start showing firing activity at Day 7. Given restraints in culturing methodology, experiments were performed on networks at least 7 days post-differentiation. The neural basal media used for the differentiating ReN cells was a DMEM/F12 GlutaMAX basal media with added B-27 supplement, heparin sodium salt, and pen-strep.

4.3 Experiments

4.3.1 Microbead Patterning

To first check the functionality of whether the bulk acoustic standing waves were created by the device, the device's ability to pattern was tested. Polymethyl Methacrylate (PMMA) microspheres (from Cospheric LLC), of diameters between 1 to 40 microns were used for testing the device's patterning capabilities. The mass concentration of the microbead in the water solution used is 0.2% and this solution is vortexed before to break up any aggregates forming within the solution. 2 ml of water is added to the plate followed by the function generator connected to the piezo plates. 1 ml of the microbead solution was then added to the petri dish and is imaged via the in-lab built multiscale microscope. The beads were dropped onto the petri dish after the device was turned on because the acoustic force is not strong enough to pattern the beads if they already reach the bottom of the petri dish.

The theoretical spacing between the arrays of beads, utilizing standing sine waves, should be in accordance with the spacing of the nodes defined by the following equation:

$$\lambda = v/f$$

The v is the speed of sound in a medium, $\lambda/2$ is the theoretical spacing between nodes and f is the frequency of the acoustic waves. The speed of sound in water, the

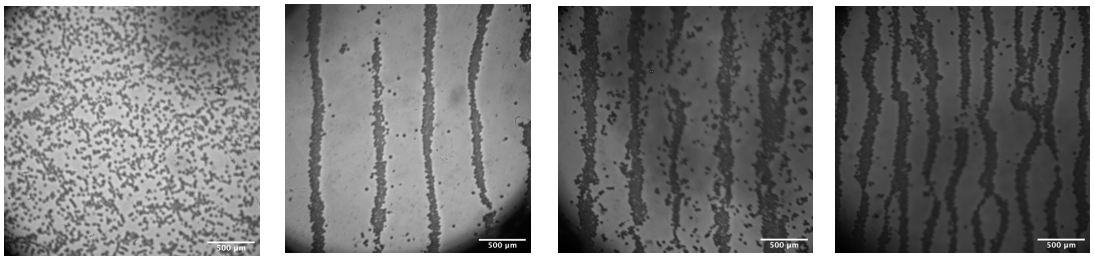

Figure 17. Representative images of microbead patterning at different frequencies and 20 Vpp. From left to right:0, 1.5, 2.04, 3.0 MHz.

medium for this demonstration, is approximately 1500 m/s. Using the plate's resonance frequency, 2.04 MHz, should yield a node spacing of approximately 367 µm. Increasing the frequency should decrease the spacing and decreasing the frequency should increase the spacing. Microbead patterning was tested at a constant 20 Vpp voltage and varied frequencies at 1.5, 2.04, 3.0MHz. Figure 17 shows representative images of microbead patterning at different frequencies.

The change in patterning follows the theoretical trend of changing frequency vs difference in spacing. The theoretical spacing, as following the equation above, should be 500, 367, and 250 microns for 1.5, 2.04, and 3.0 MHz respectively. The exact values of spacing seen in Table 1, however, did not exactly match the theoretical spacing. This can potentially be explained by the fact that the standing waves may also be moving the water into certain patterns. Such flowing patterns of

the water may distort the bead patterning into some curved lines rather than all straight lines. Additionally, the ultrasound waves may have been attenuated by the printed resin separating the plate and cell media. However, for the scope of this project, the device was able to form standing waves that can pattern beads.

Measurement	1.5 MHz	2.04 MHz	3.0 MHz
1	572.507	485.631	220.361
2	559.647	461.345	215.715
3	539.005	461.406	217.363
4	567.809	470.156	270.917
5	572.974	450.677	254.084
Average	562.388	465.843	235.688

Table 1. Spacing between beads at different applied frequencies in microns. The 5 measurements taken of each frequency were calculated as the average spacing at 5 different latitudinal sections.

4.3.2 Neural Network Experiments

To sterilize the device, it was sprayed with 70% ethanol, set to dry, and was exposed to UV light in a cell culture hood. As mentioned earlier, ReN human neural progenitor stem cells(hNPCs) were plated onto laminin coated petri dishes at 3 x 10^5 densities. These plated cells were then set to differentiate from 7 to 14 days. Full differentiation occurs at Day 14, but activity is visible at Day 7. The ReN cells were then incubated with a Calbryte 590 for one hour before having its media replaced with 1 ml of fresh media. The petri dish was placed in the incubated stage on the multiscale with the incubator set at 37℃ and 5% CO2 flow. The device was then placed into the petri dish with its wiring lead out of the incubator and connected to the function generator. The function generator was set to produce sinusoidal waves at the piezo plate's resonance frequency 2.04 MHz. Figure 18 shows this set-up. The experiments were then run by recording at 3 frames per second and 333 ms exposure

time. The recording was done via the widefield method that contains a 561 nm excitation laser. The petri dishes were recorded for a period with the device turned on in the middle of the recording to identify whether there was any change in activity with implementation of the acoustic waves.

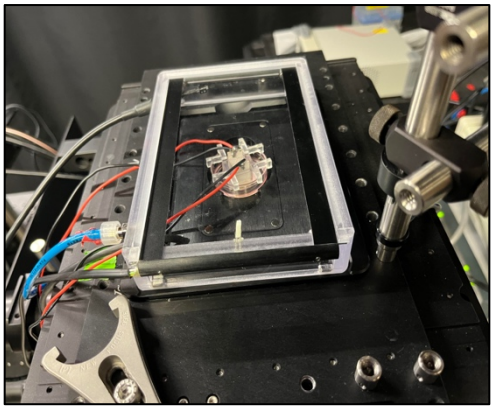

Figure 18. Experimental setup of device on petri dish in imaging incubator of the multiscale microscope.

4.3 Analysis

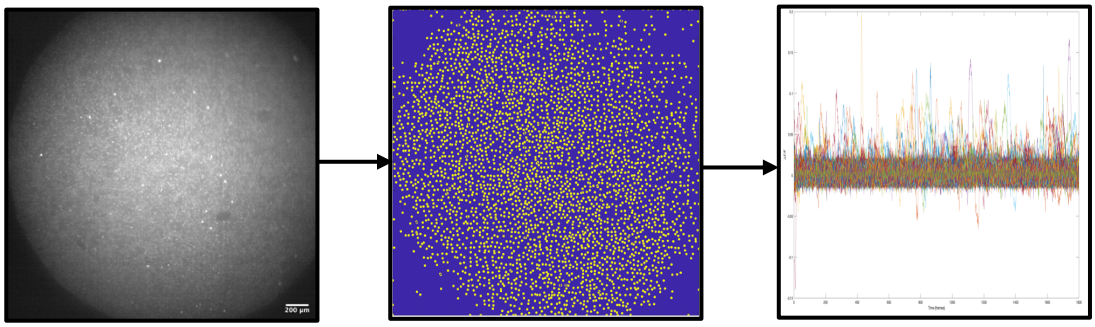

Figure 19. Schematic of how analysis was conducted. Entire videos (left) were processed and cell centers + radius were identified within the video (center). The ΔF/F traces were then obtained for each cell over the course of time (right).

To analyze the recorded videos, an in-lab built MATLAB script was used to identify individual cells and track their change in fluorescence over time. To identify individual cells, two separate differences of gaussian (DOG) filters were applied to the recorded video. The two filtered videos are then subtracted from each other with the resultant video highlighting the borders of individual cell bodies. A pre-selected

cell radius, determined manually to be about 8 pixels, is used to create cells of these sizes. The bottom 75% of values from a selection of 40 frames of the recorded video is used to determine the baseline fluorescence of each individual cell. Each cell's change in fluorescence relative to its baseline value is calculated per recorded frame and is stored in a variable DFF(also known as ΔF/F). Figure 19 shows an overview of how the ΔF/F traces were obtained from the recorded videos. To reduce the impact of noise on results only active cells were used for analysis. Active cells were filtered for utilizing the findpks function in MATLAB. A moving average of 5 was used to smooth out the traces and peak detection occurred for peaks with prominence of greater than three times the standard deviation above the average ΔF/F and of pk heights greater than 0.03. Cells that had greater than 3 peaks per video were designated as active.

Once the active cell ΔF/F traces were obtained for each video, they were first split into three sections. These three sections being when the device was off, when the device was turned on and when the device was turned off again. Within each section, each trace was integrated and summed up to obtain the total change in fluorescence for the entire dish. To normalize this total change in fluorescence between plates, which differ in cell population, and each section duration, the summed integrated ΔF/Fs were divided by the number of cells and number of frames. The integrated ΔF/Fs serve as a quantitative number to indicate the overall activity strength level of a given plated neural network. The second metric measured in the recordings was spikes per minute which is a measure for activity frequency. This was done by summing up the number of spikes for each cell within the measured period and

dividing that number by the duration of the period in minutes. The spike frequency was additionally normalized by the number of cells to make the results between different plates comparable. The spikes per minute per cell is measured because it serves as a metric of how often neuron reach an action potential.

4.4 Results

4.4.1 Day 7 (D7) Differentiated Plates

Acoustic forcing was first applied to Day 7 differentiated neural network. The plate was recorded for nine minutes with minute four through six being the time in which acoustic forcing was applied. Figure 20 shows the heat map of the neural network's active cells during the entire nine-minute recording. The right figure

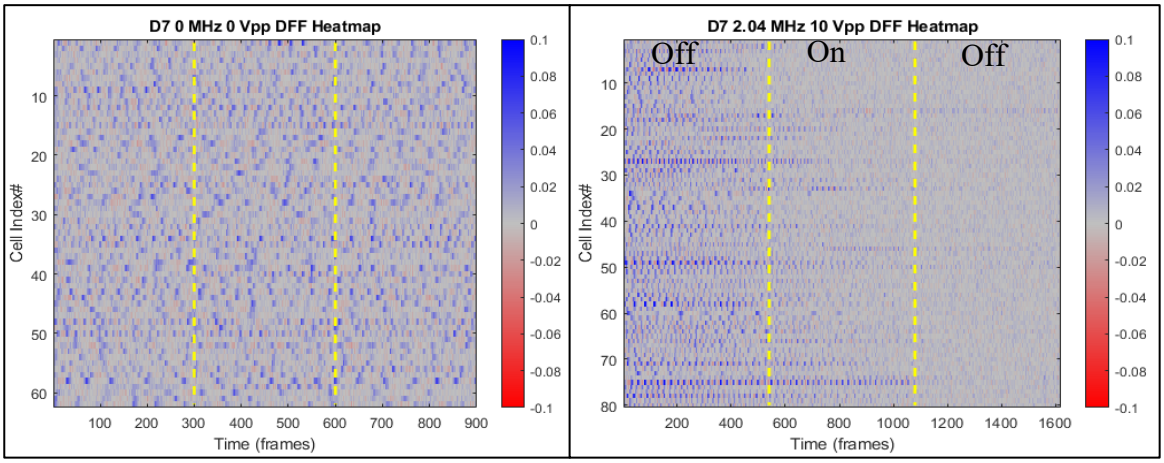

Figure 20. ΔF/F heatmaps of Day 7 differentiated active cells when exposed to acoustic forcing. The blue represents increases in ΔF/F while the red represents decreases in ΔF/F. The ΔF/F traces of cells in the control group (left) with no acoustic forcing and experimental group with acoustic force of 10 Vpp & 2.04 MHz (right are shown). The section between the yellow lines in the experimental group represents the time when acoustic forcing is on. There is a noticeable decrease in positive fluorescence spikes during and after the acoustic forcing application.

specifically shows the ΔF/F heat map of active cells with acoustic forcing applied between frames 540 and 1080. There is a noticeable decrease in ΔF/F values during and after the application of acoustic forcing at 2.04 MHz and 10 Vpp. The left

heatmap in Figure 20 represents the ΔF/F traces of active cells in the same Day 7 plate but in a different field of view with no acoustic forcing applied to serve as a control. It was recorded for five minutes and split into three equal sections to be comparable to the acoustic forcing group's traces.

From the obtained traces of each active cell, the overall change in fluorescence- normalized by the number of frames and cells, and the number of fluorescence spikes- were recorded before, during, and after acoustic forcing application. The scatter plots in Figure 21 show the integrated ΔF/F per frame for each cell (left) and the spike frequency for each individual cell (right). The axes represent the status of acoustic forcing: the initial absence of acoustic forcing (Device Off), the application of acoustic forcing (Device On), and forcing turn off (Device Off2). The cells within the petri dish that experienced acoustic forcing (red) can be seen, in the Device Off to Device On transition, generally along the Device Off axis which indicates that its highest values were in the Device Off condition comparative to the Device On period. The cells are seen closer along the Device On axis compared to the Device Off2 axis in the acoustic forcing to no forcing in the second transition. This indicates the general trend of cells experiencing a decrease in fluorescence and spike activity from Device On to Device Off status. The control group of cells that did not experience any acoustic forcing are more evenly distributed along all y=x function which indicates that its values do not significantly differ over time.

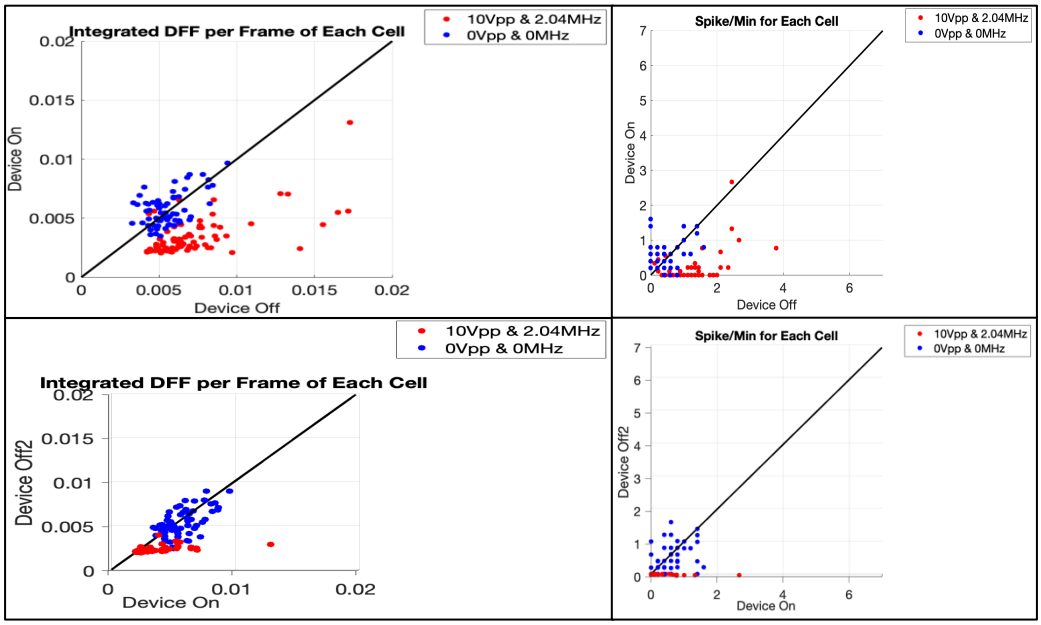

Figure 21. Scatter plot representing the total average fluorescence change per cell from before to during acoustic forcing (top left) and from during acoustic forcing to after (bottom left). The corresponding spike per minute frequency for each transition is shown on the right.

Figure 22 displays an average of individual cell fluorescence and spike activity value and represents them as bar charts. There is a 52.77% decrease in the integrated ΔF/F value from the pre-acoustic forcing to acoustic forcing and then a 32.35% decrease from acoustic forcing to post-acoustic forcing. The number of spikes also decreased by 85.56% from pre-acoustic forcing to acoustic forcing and then 100% from acoustic forcing to post-acoustic forcing. For the control group, there was an increase of 5.45% in integrated ΔF/F from the first to second period and a 6.89% decrease from the second to third period. The spike frequency increased

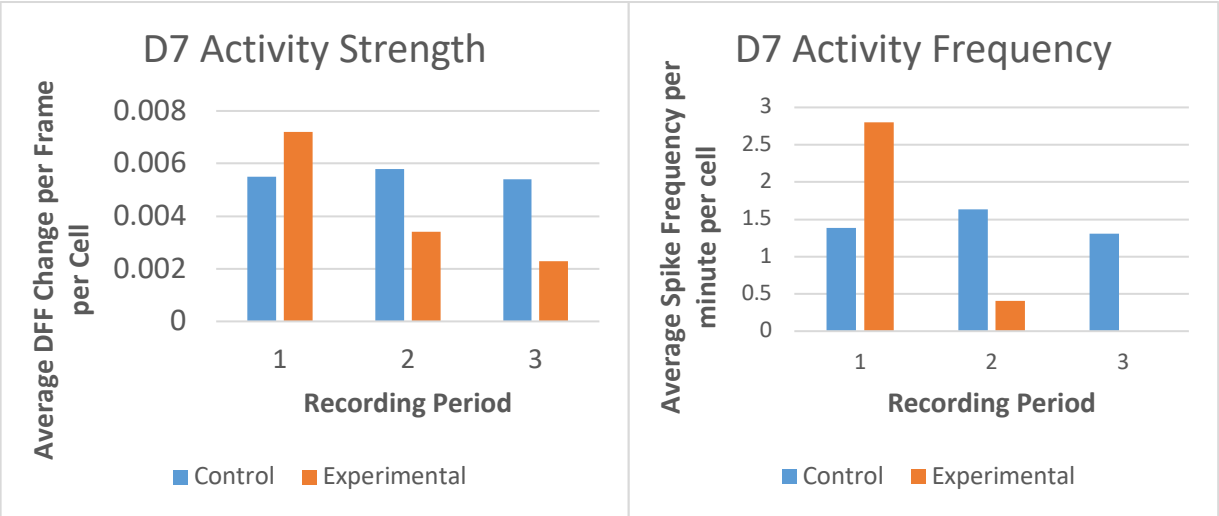

Figure 22. The bar chart (left) shows average fluorescence change per cell per frame and the bar chart (right) shows the spike frequency. Acoustic forcing was applied during recording period 2 in the experimental group. A noticeable decrease in DFF and spike frequency is seen in the recording after applying acoustic forcing.

18.18% for the first to second period and then decreased 20.11% for the second to third period transition.

4.4.2 Day 8 (D8) Differentiated Plates

To further clarify whether the change in activity strength and frequency was due to acoustic forcing application or not, the duration of acoustic forcing application was altered. The cells were recorded for 10 minutes with the first three minutes without acoustic forcing, the next two minutes with acoustic forcing at 2.04 MHz & 10 Vpp, and the last five minutes without acoustic forcing. The network's active cells ΔF/F heatmap traces can be found on the right side in Figure 22. The data between frames 540 and 900 represent the period in which acoustic forcing is applied. An additional five-minute recording was done on a different field of view within the same plate but without any acoustic forcing application to serve as the control. The ΔF/F heatmap for this recording can be seen on the left side of Figure 23.

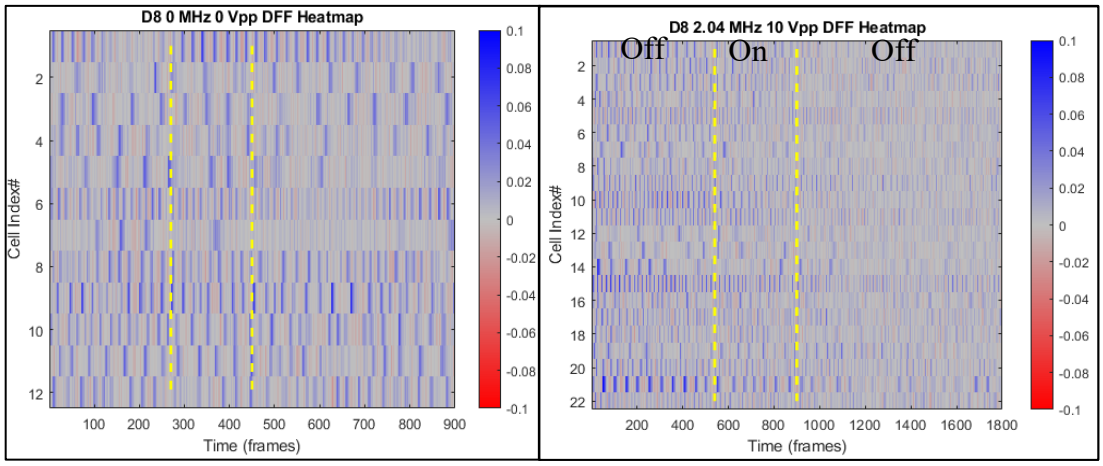

Figure 23. The ΔF/F traces of cells in the control group (left) with no acoustic forcing and experimental group with acoustic force of 10 Vpp & 2.04 MHz (right are shown). The section between the yellow lines in the experimental group represents the time when acoustic forcing is on. There is noticeable decrease in fluorescence after application of acoustic field.

The scatter plots in Figure 24 represent the individual cells integrated ΔF/F(left) and spike frequency(right) with respect to activation/inactivation of acoustic forcing. The scatter plots for total fluorescence change and spike frequency were split by plotting the cell values with axes of Device Off/Device On and Device On/Device Off2. This was done to show the difference in activity between the acoustic force application transition. The 10 Vpp & 2.04 MHz group has a general shift toward the initial Device Off axis which indicates higher ΔF/F and spike frequency values prior to acoustic forcing. This is once again seen in the Device On/Device Off2 axis graphs. A y = x line was plotted in each scatter plot as a reference mark to what

values would be considered equal between two conditions.

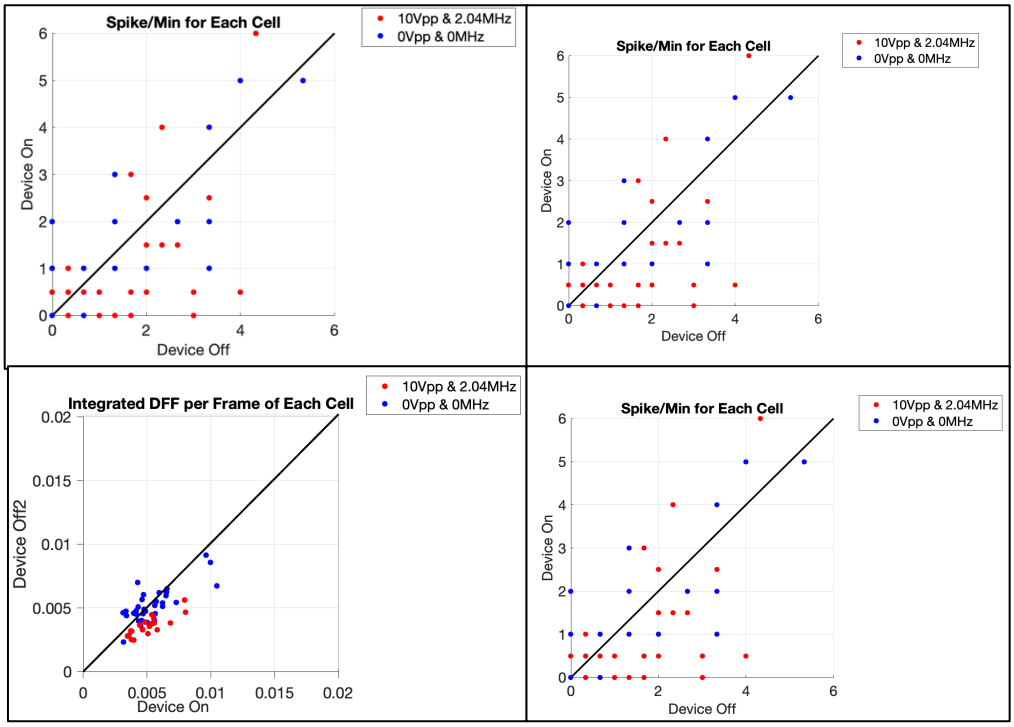

Figure 24. Scatter plot representing the total average fluorescence change per cell from before to during acoustic forcing (top left) and from during acoustic forcing to after (bottom left). The corresponding spike per minute frequency for each transition is shown on the right. The y = x line is plotted for reference to show what equal values between each axis would be.

Figure 25 shows the average fluorescence change and spike frequency per cell during each phase of this plate recording. The cells in the experimental group expressed a 23.18% decrease in average fluorescence from pre-acoustic to acoustic forcing period and a 33.96% decrease from acoustic to post-acoustic forcing period. The spike frequency decreased by 15.5% and 78.42% respectively. The control saw a 3.84% increase in average ΔF/F from the first to second period and a 5.55% decrease during the second to third period transition. The spike frequency change was an 8.61% increase and then an 8.57% decrease from the first to second and second to third transition respectively.

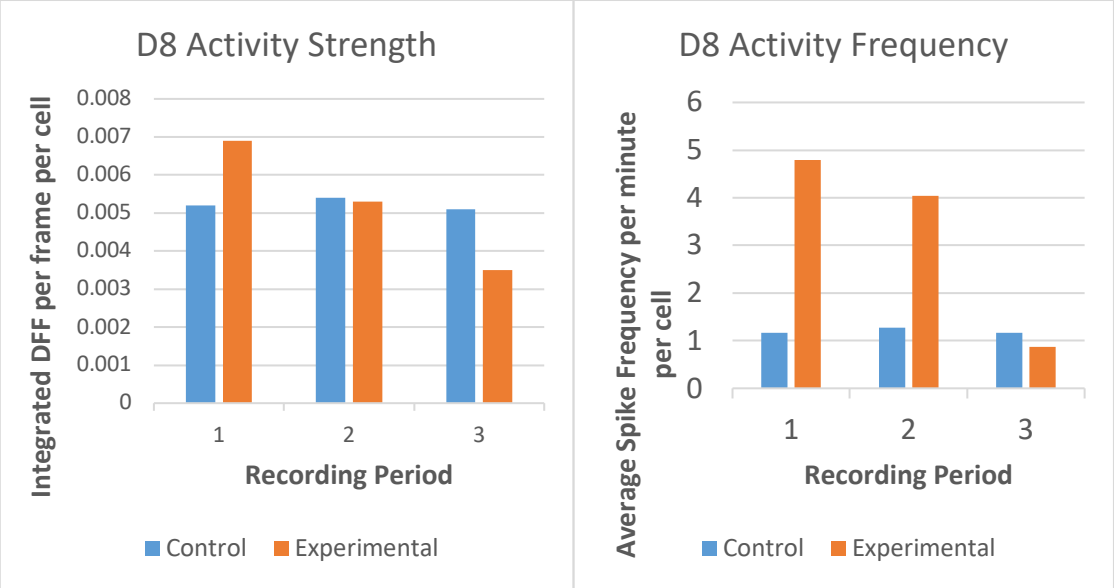

Figure 25. The bar chart (left) shows the integrated average fluorescence change per cell per frame in each experimental condition with and without acoustic forcing. The bar chart (right) shows the summed spike frequency during acoustic forcing. Acoustic forcing was applied during recording period 2 in the experimental group. A noticeable decrease in DFF and spike frequency is seen in the recording after applying acoustic forcing.

4.4.3 Day 14 (D14) Differentiated Plates

The hNPC derived neural networks start to show activity after 7-day differentiation but are considered mature at 14-day differentiation. Thus, acoustic forcing was applied to a 14-day differentiated network at 2.04 MHz and 10 Vpp. The recording was done for nine minutes with acoustic forcing applied minutes four to six. A control plate, separate from the plate exposed to acoustic forcing but from the same

growing flask, was also recorded for nine minutes to serve as the control. Figure 26 shows the ΔF/F heatmap traces of the control and the acoustic forced neural network.

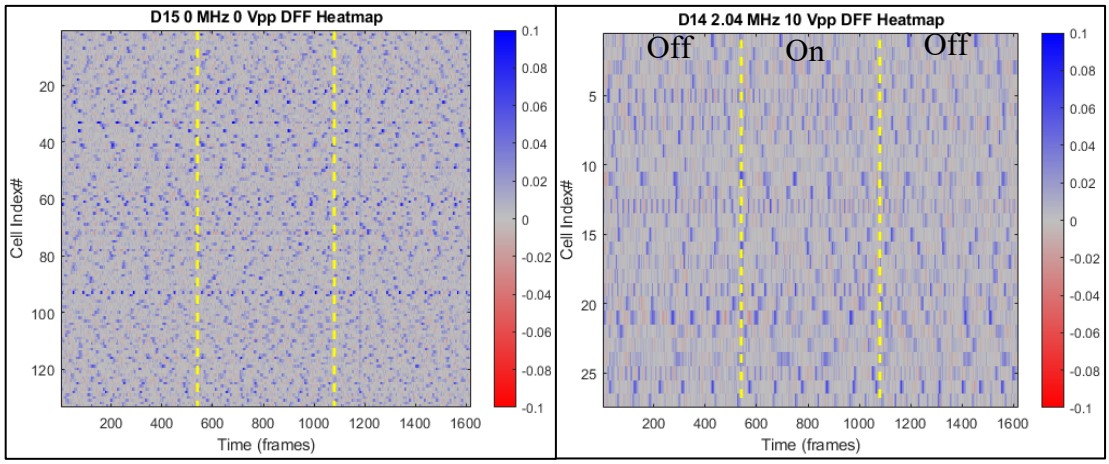

Figure 26.ΔF/F heatmaps of active cells when exposed to acoustic forcing. The ΔF/F traces of cells in the control group (left) with no acoustic forcing and experimental group with acoustic force of 10 Vpp & 2.04 MHz (right). The section between the yellow lines in the experimental group represents the time when acoustic forcing is on.

Figure 27 shows the total average fluorescence change (left) and spike frequency(right) for this plate recording during each period for each cell. The scatter plots are split into showing the values in the initial off to on switch of acoustic force and the on to off switch. Figure 28 shows the values for ΔF/F and spike frequency summed for all cells. The cells expressed a 1.88% decrease in average fluorescence from pre-acoustic to acoustic forcing period and a 3.84% decrease from acoustic to post-acoustic forcing period. The spike frequency decreased by 13.26% and 5.87% respectively. The control saw a 1.88% increase in average ΔF/F from the first to second period and a 3.70% decrease during the second to third period. The spike frequency change was a 3.63% decrease and then a 5.38% decrease.

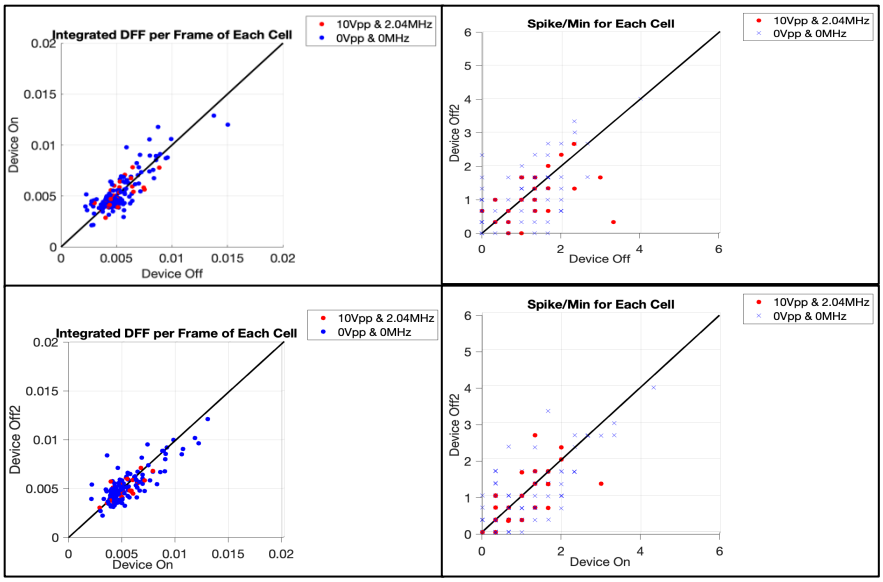

Figure 27. Scatter plot representing the total average fluorescence change per cell from before to during acoustic forcing (top left) and from during acoustic forcing to after (bottom left). The corresponding spike per minute frequency for each transition is shown

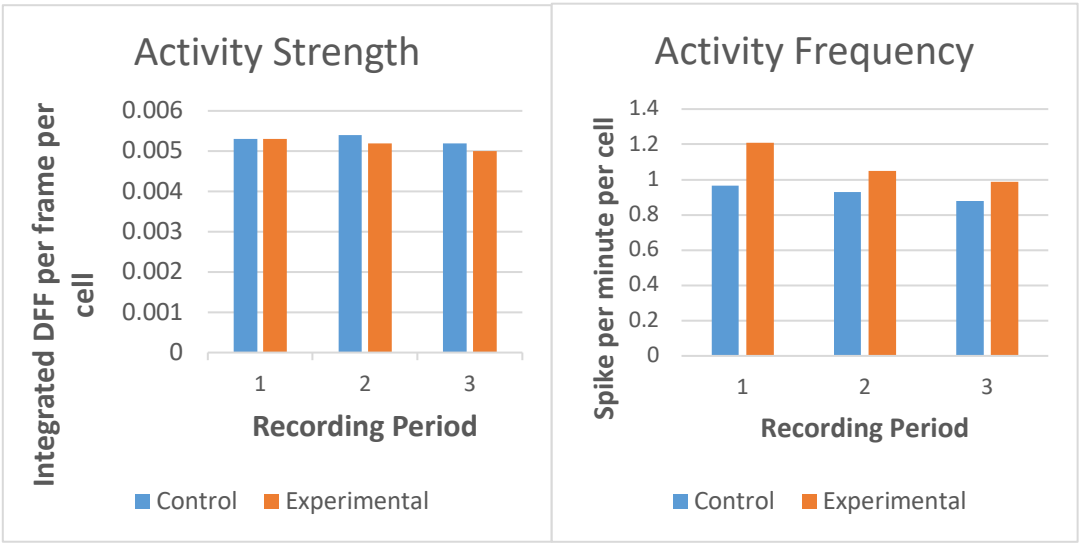

Figure 28. The left bar chart shows integrated average fluorescence change per cell per frame in each experimental condition with and without acoustic forcing. The right bar chart shows the spike frequency during acoustic voltage of varying voltage. Acoustic forcing was applied during recording period 2 in the experimental group. No noticeable change in DFF and spike frequency is seen in the recording after applying acoustic forcing.

4.4.4 Varying Voltage in Mature Networks

To evaluate the impact of changing voltage on network activity, acoustic forcing was applied on a day 14 differentiated network. It was recorded at the same

field of view (FOV) for different voltages: 1, 10, and 20 Vpp at the same 2.04 MHz frequency. Figure 29 shows the ΔF/F heatmap traces for active cells during the entire recording. Acoustic forcing was applied for minute four to six of the nine-minute recording. Table 2 shows the calculated ultrasound at each tested voltage as described in the methodology.

	1 Vpp	**10 Vpp**	**20 Vpp**
Intensity	0.019 W/cm^2	1.905 W/cm^2	7.620 W/cm^2

Table 2. Ultrasound intensity of each tested voltage.

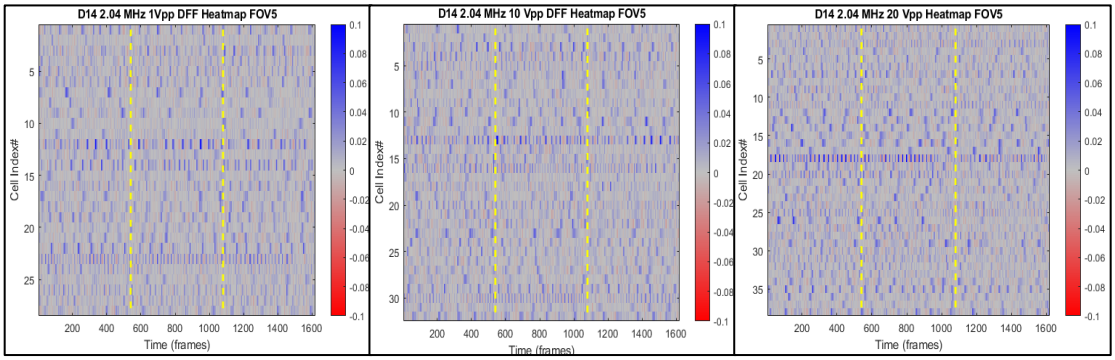

Figure 29. The heatmaps of cell ΔF/F traces in the same field of view at varying voltages: 1 Vpp (left), 10 Vpp (center), and 20 Vpp (right) at the same 2.04 MHz frequency. The section between the two dotted yellow lines represents the time during which the device is on.

Figure 30 depicts integrated ΔF/F and spike frequency for each cell total average fluorescence change per frame with and without acoustic forcing as scatter plots. They are split, like the previous scatter plots, into the first transition of acoustic forcing being turned on and the second transition of acoustic forcing being turned off.

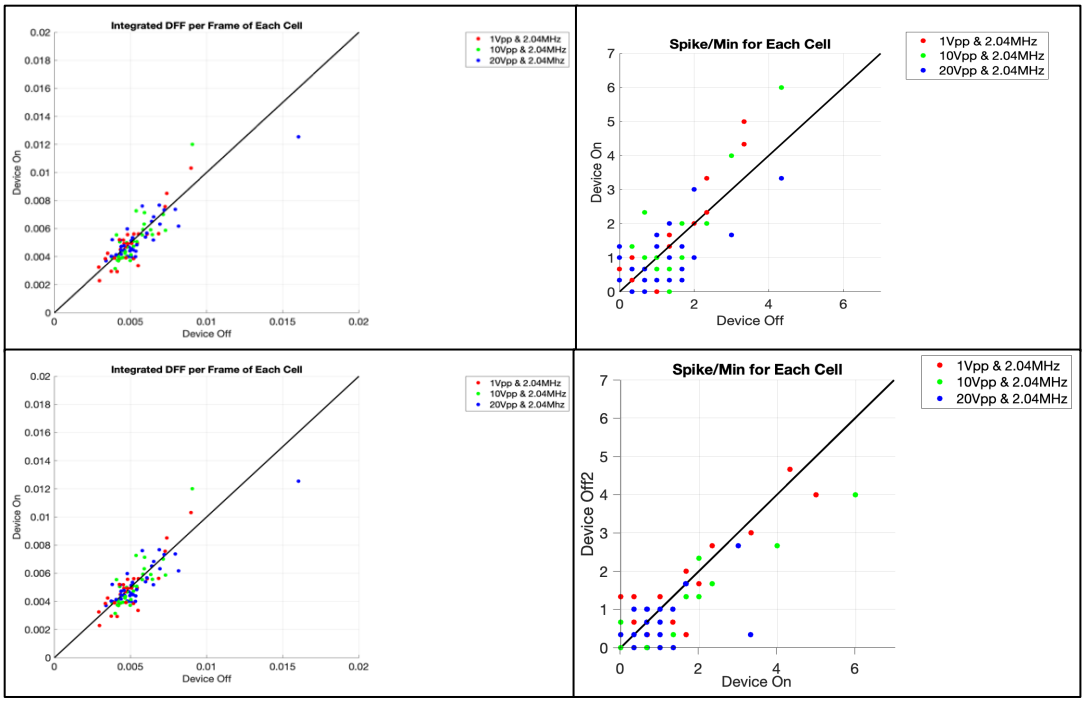

Figure 30. The top scatter plots show the integrated ΔF/F values for individual cells (left) and spike frequency of each cell (right) in each device condition. The left bar chart shows average fluorescence change per cell per frame in each experimental condition

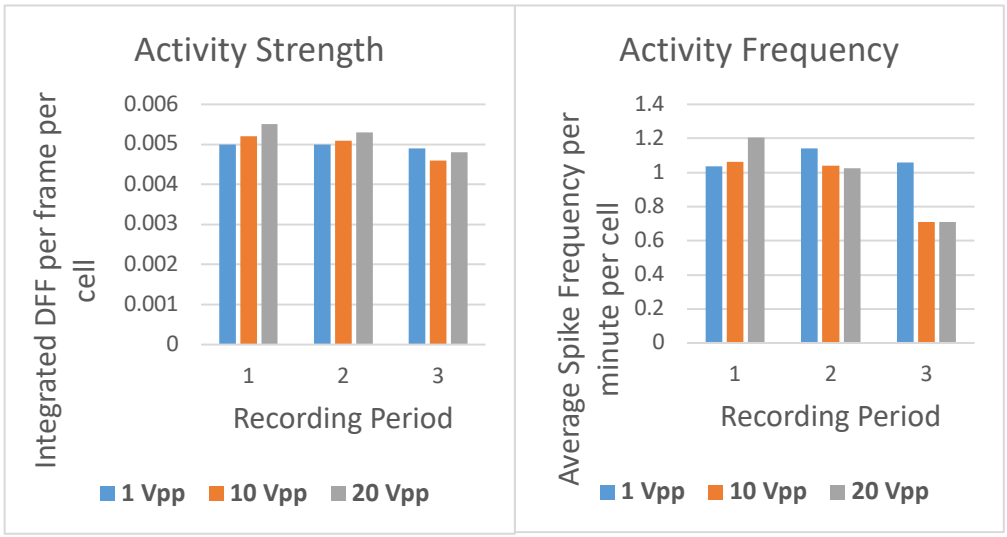

Figure 31. The right bar chart shows the spike frequency during acoustic voltage of varying voltage. These were both recorded from Day 14 differentiated plate on the same FOV. The left bar chart shows average fluorescence change per cell per frame in each experimental condition with and without acoustic forcing. The right bar chart shows the spike frequency during acoustic voltage of varying voltage.

Figure 31 shows the ΔF/F and spike frequency summed over each cell in each device condition. The 1 Vpp acoustic forcing group saw no change in average

fluorescence change from pre-forcing to forcing and then a 2% decrease between forcing and post-forcing. The spike frequency increased 10.35% and decrease 7.29% respectively. The 10 Vpp acoustic forcing saw a decrease in total average ΔF/F of 1.92% and 9.80% and an initial decrease in spike frequency of 1.95% followed by a decrease of 32.01%. The 20 Vpp saw a decrease in fluorescence change of 3.63% and 9.43% and a decrease in spike frequency of 14.92% and 30.77%.

4.5 Discussion

From the above data, the less differentiated networks (D7 and D8) showed a significant decrease in neuronal activity indicated by the large decrease in change of fluorescence and in the frequency of spikes when exposed to acoustic forcing. These values proceeded to decrease after acoustic forcing application as well. Both metrics represent how active the cells are and to what degree they are active. Larger increases in fluorescence indicate a stronger action potential, via Ca^{+2} entry, while the spike frequency indicates how often a cell is reaching action potential. Recordings and analysis of the plates were conducted without turning the device on. This was done to show whether the presence of the device itself affected neuronal calcium activity. However, this was not the case with the ΔF/F and spike frequency values staying relatively unchanged throughout the recording compared to the acoustic forcing trials. A potential reason for the decrease in activity may be attributed with the death of the neuronal cells. However, cellular apoptosis is associated with large influxes of calcium[74,75]. The calcium influx in such a situation is not transient and so the Calbryte dye would remain in the dead cell. This would show as a continuous positive ΔF/F spike which is not seen in the ΔF/F heatmaps. Another potential reason for decreased

activity is the applied wave had a 100% duty cycle. This constant stimulation may have produced enough heat to disrupt the Ca^{+2} mechanosensitive channels involved in neuronal activity[51]. Reducing the duty cycle in future experiments would help elucidate the impact of constant stimulation. Another alternative explanation is that the application of acoustic forcing pushes neurotransmitters in the media into vortices generated by the standing waves. This may prevent neurotransmitters from reaching their targeted neurons and thus lower the amount of network activity.

When investigating more mature and differentiated network (D14) showed a much less noticeable change in $\Delta F/F$ and spike frequency with exposure to acoustic forcing. A control plate with cells from the same culturing flask was recorded for the same duration of time without any acoustic forcing. This was done to verify that the mere presence of the device alters calcium activity. The integrated fluorescence changes and spike frequency remains stable throughout the recording. However, one point of note for this petri dish is that the cells were much more clumped together than the previously tested dishes. This blurs the reasoning as to why the network activity is not impacted by acoustic forcing application whether it be the clumping or age/differentiation of cells. Repeated replicates need to be done to verify whether the clumping of cells is what mitigated the impact of acoustic forcing on cell activity. A potential explanation for this observation is that the distance that neurotransmitters need to travel before reaching their targeted cell is less in the clumped network. Thus, the standing wave induced vortices picking up neurotransmitters may not as significant in regulating neural network activity.

The last experiment focused on whether changing the intensity, via the voltage output from the function generator, changes the resulting neuronal activity. The application of 1 Vpp acoustic wave did not appear to have any impact on average fluorescence change and frequency. The 10 Vpp and 20 Vpp conditions both saw minimial changes in overall fluorescence change and a decrease in spike frequency. This potentially could be explained by the trend that higher intensities elicit a larger increase in thermal energy. The larger increase in thermal energy surrounding the cells may distress their mechanosensitive calcium channels and limit their signaling activity. Alternatively, only higher intensities may be able to form acoustic streaming vortices within the media that could be keeping neurotransmitters from reaching their target cells and mitigating network activity.

To summarize, the application of acoustic forcing looked to decrease neuronal activity while the older mature networks' activity did not seem to be impacted impact as greatly. The use of higher voltage, 10 and 20 Vpp, looked to have negatively impact spike frequency. Future directions from this work should focus on conducting replicates for the previously mentioned experiments. Additionally, metrics indicative of neuronal activity should be measured including cell voltage and correlation matrices of cells. Additional future directions can also compare cell activity located in nodal regions to cell activity in anti-nodal regions.

4.6 Conclusion

Neural network research is an increasingly popular research field at the intersection of neuroscience and bioengineering. Studying how such networks function and fabricating more complex networks to represent in vivo-like neural

structures provides great potential for understanding how neurological disorders occur and potential treatments. Acoustic forcing is a particular phenomenon that has been heavily utilized in neural network research. Acoustic forcing is the phenomenon in which acoustic waves transfer energy when interacting with an object/medium to induce a force on said object/medium. Acoustic forcing, specifically utilizing standing ultrasonic waves, has previously been utilized successfully in cell patterning to form in-vivo like neural structures such as cerebral cortices, and for neuromodulation to modulate neuron activity. However, the impact of these standing acoustic waves has on neural network activity is not clear. Such a piece of information is needed to understand more about how standing waves, which occur in trans-cranial focused ultrasound, can impact neuronal activity.

For this thesis, a device was fabricated produce standing acoustic waves. Its ability to produce such waves was verified by its ability to pattern microbeads. Utilizing this device, acoustic standing waves are applied to a hNPC derived neural network and are assessed for activity with and without acoustic forcing. From these preliminary findings, younger and less differentiated networks show a decrease in activity when exposed to acoustic forcing while the older and more differentiated networks show a smaller difference in neuronal activity when exposed to acoustic forcing. This could potentially point out that ReN cell-based networks need to be fully differentiated before perturbation with acoustic forcing. The ultrasound intensities at higher intensities looked to have a slightly more inhibitory effect on neuronal activity comparative to lower intensities. Future works should first repeat the current study for more replicates to ensure validity. After this, other metrics of

neuronal activity, cell membrane potential, should be measured and ultrasound wave parameters, such as frequency and duty cycle, should be modulated.

Bibliography

1. Leighton, T. G. What is ultrasound? *Progress in Biophysics and Molecular Biology* **93**, 3–83 (2007).
2. Berger, A. Echocardiography. *BMJ* **321**, 218 (2000).
3. Yiannacou, K. & Sariola, V. Acoustic Manipulation of Particles in Microfluidic Chips with an Adaptive Controller that Models Acoustic Fields. *Advanced Intelligent Systems* **5**, 2300058 (2023).
4. Van Schependom, J. & D'haeseleer, M. Advances in Neurodegenerative Diseases. *J Clin Med* **12**, 1709 (2023).
5. O'Reilly, M. A., Huang, Y. & Hynynen, K. Impact of standing wave effects on transcranial focused ultrasound disruption of the blood-brain barrier in a rat model. *Phys Med Biol* **55**, 5251–5267 (2010).
6. Olson, J. L., Atala, A. & Yoo, J. J. Tissue Engineering: Current Strategies and Future Directions. *Chonnam Med J* **47**, 1–13 (2011).
7. Kačarević, Ž. P. *et al.* An Introduction to 3D Bioprinting: Possibilities, Challenges and Future Aspects. *Materials (Basel)* **11**, 2199 (2018).
8. Mani, M. P. *et al.* A review on 3D printing in tissue engineering applications. *Journal of Polymer Engineering* **42**, 243–265 (2022).
9. Agarwal, S. *et al.* Current Developments in 3D Bioprinting for Tissue and Organ Regeneration–A Review. *Front. Mech. Eng.* **6**, (2020).
10. Jentsch, S. *et al.* Multiscale 3D Bioprinting by Nozzle-Free Acoustic Droplet Ejection. *Small Methods* **5**, 2000971 (2021).
11. Guo, Q. *et al.* A review on acoustic droplet ejection technology and system. *Soft Matter* **17**, 3010–3021 (2021).
12. Wang, J. *et al.* Rational Design and Acoustic Assembly of Human Cerebral Cortex-Like Microtissues from hiPSC-Derived Neural Progenitors and Neurons. *Adv Mater* **35**, e2210631 (2023).
13. Bouyer, C. *et al.* A Bio-Acoustic Levitational (BAL) Assembly Method for Engineering of Multilayered, 3D Brain-Like Constructs, Using Human Embryonic Stem Cell Derived Neuro-Progenitors. *Advanced Materials* **28**, 161–167 (2016).
14. Cohen, S. *et al.* Large-scale acoustic-driven neuronal patterning and directed outgrowth. *Sci Rep* **10**, 4932 (2020).
15. Armstrong, J. P. K. *et al.* Engineering Anisotropic Muscle Tissue using Acoustic Cell Patterning. *Advanced Materials* **30**, 1802649 (2018).
16. Kang, B. *et al.* High-resolution acoustophoretic 3D cell patterning to construct functional collateral cylindroids for ischemia therapy. *Nat Commun* **9**, 5402 (2018).
17. Sun, C. *et al.* Acoustically accelerated neural differentiation of human embryonic stem cells. *Acta Biomaterialia* **151**, 333–345 (2022).
18. Ambattu, L. A., Gelmi, A. & Yeo, L. Y. Short-Duration High Frequency MegaHertz-Order Nanomechanostimulation Drives Early and Persistent Osteogenic Differentiation in Mesenchymal Stem Cells. *Small* **18**, 2106823 (2022).

19. Cooper, J. M. Challenges in lab-on-a-chip technology. *Frontiers in Lab on a Chip Technologies* **1**, (2022).
20. S. Mielczarek, W., A. Obaje, E., T. Bachmann, T. & Kersaudy-Kerhoas, M. Microfluidic blood plasma separation for medical diagnostics: is it worth it? *Lab on a Chip* **16**, 3441–3448 (2016).
21. Liu, S. C., Yoo, P. B., Garg, N., Lee, A. P. & Rasheed, S. A microfluidic device for blood plasma separation and fluorescence detection of biomarkers using acoustic microstreaming. *Sensors and Actuators A: Physical* **317**, 112482 (2021).
22. Nyborg, W. L. Ultrasonic microstreaming and related phenomena. *Br J Cancer Suppl* **5**, 156–160 (1982).
23. Li, P. *et al.* Acoustic separation of circulating tumor cells. *Proc Natl Acad Sci U S A* **112**, 4970–4975 (2015).
24. Ding, X. *et al.* Cell separation using tilted-angle standing surface acoustic waves. *Proc Natl Acad Sci U S A* **111**, 12992–12997 (2014).
25. Doherty, J. R., Trahey, G. E., Nightingale, K. R. & Palmeri, M. L. Acoustic Radiation Force Elasticity Imaging in Diagnostic Ultrasound. *IEEE Trans Ultrason Ferroelectr Freq Control* **60**, 685–701 (2013).
26. Wu, M. *et al.* Acoustofluidic separation of cells and particles. *Microsyst Nanoeng* **5**, 1–18 (2019).
27. J. Delaney, L., Isguven, S., R. Eisenbrey, J., J. Hickok, N. & Forsberg, F. Making waves: how ultrasound-targeted drug delivery is changing pharmaceutical approaches. *Materials Advances* **3**, 3023–3040 (2022).
28. Correas, J.-M. *et al.* Ultrasound contrast agents: properties, principles of action, tolerance, and artifacts. *Eur Radiol* **11**, 1316–1328 (2001).
29. Postema, M., van Wamel, A., Lancée, C. T. & de Jong, N. Ultrasound-induced encapsulated microbubble phenomena. *Ultrasound Med Biol* **30**, 827–840 (2004).
30. Daneman, R. & Prat, A. The Blood–Brain Barrier. *Cold Spring Harb Perspect Biol* **7**, a020412 (2015).
31. Mehta, R. I. *et al.* Ultrasound-mediated blood–brain barrier opening uncovers an intracerebral perivenous fluid network in persons with Alzheimer's disease. *Fluids and Barriers of the CNS* **20**, 46 (2023).
32. McDannold, N., Arvanitis, C. D., Vykhodtseva, N. & Livingstone, M. S. Temporary Disruption of the Blood–Brain Barrier by Use of Ultrasound and Microbubbles: Safety and Efficacy Evaluation in Rhesus Macaques. *Cancer Research* **72**, 3652–3663 (2012).
33. Gasca-Salas, C. *et al.* Blood-brain barrier opening with focused ultrasound in Parkinson's disease dementia. *Nat Commun* **12**, 779 (2021).
34. Jain, R. K. Determinants of Tumor Blood Flow: A Review1. *Cancer Research* **48**, 2641–2658 (1988).
35. Goertz, D. E. *et al.* Antitumor Effects of Combining Docetaxel (Taxotere) with the Antivascular Action of Ultrasound Stimulated Microbubbles. *PLOS ONE* **7**, e52307 (2012).
36. Geers, B., Dewitte, H., De Smedt, S. C. & Lentacker, I. Crucial factors and emerging concepts in ultrasound-triggered drug delivery. *J Control Release* **164**, 248–255 (2012).

37. Chowdhury, S. M., Abou-Elkacem, L., Lee, T., Dahl, J. & Lutz, A. M. Ultrasound and microbubble mediated therapeutic delivery: Underlying mechanisms and future outlook. *J Control Release* **326**, 75–90 (2020).
38. Delaney, L. J. *et al.* Gemcitabine-loaded microbubble system for ultrasound imaging and therapy. *Acta Biomater* **130**, 385–394 (2021).
39. Wang, H. & Jasim, A. 14 - Piezoelectric energy harvesting from pavement. in *Eco-Efficient Pavement Construction Materials* (eds. Pacheco-Torgal, F., Amirkhanian, S., Wang, H. & Schlangen, E.) 367–382 (Woodhead Publishing, 2020). doi:10.1016/B978-0-12-818981-8.00014-X.
40. Quarato, C. M. I. *et al.* A Review on Biological Effects of Ultrasounds: Key Messages for Clinicians. *Diagnostics (Basel)* **13**, 855 (2023).
41. Rasouli, R., Villegas, K. M. & Tabrizian, M. Acoustofluidics – changing paradigm in tissue engineering, therapeutics development, and biosensing. *Lab Chip* **23**, 1300–1338 (2023).
42. Li, H. *et al.* Chapter Fourteen - Electromechanical Brillouin scattering. in *Semiconductors and Semimetals* (eds. Eggleton, B. J., Steel, M. J. & Poulton, C. G.) vol. 110 287–311 (Elsevier, 2022).
43. Go, D. B., Atashbar, M. Z., Ramshani, Z. & Chang, H.-C. Surface acoustic wave devices for chemical sensing and microfluidics: a review and perspective. *Anal. Methods* **9**, 4112–4134 (2017).
44. Zhang, Y. *et al.* Optofluidic Device Based Microflow Cytometers for Particle/Cell Detection: A Review. *Micromachines (Basel)* **7**, 70 (2016).
45. Mazalan, M. B., Noor, A. M., Wahab, Y., Yahud, S. & Zaman, W. S. W. K. Current Development in Interdigital Transducer (IDT) Surface Acoustic Wave Devices for Live Cell In Vitro Studies: A Review. *Micromachines (Basel)* **13**, 30 (2021).
46. Yang, Y., Dejous, C. & Hallil, H. Trends and Applications of Surface and Bulk Acoustic Wave Devices: A Review. *Micromachines (Basel)* **14**, 43 (2022).
47. Leibacher, I., Reichert, P. & Dual, J. Microfluidic droplet handling by bulk acoustic wave (BAW) acoustophoresis. *Lab Chip* **15**, 2896–2905 (2015).
48. Acheta, J., Stephens, S. B. Z., Belin, S. & Poitelon, Y. Therapeutic Low-Intensity Ultrasound for Peripheral Nerve Regeneration – A Schwann Cell Perspective. *Front. Cell. Neurosci.* **15**, (2022).
49. Elhelf, I. A. S. *et al.* High intensity focused ultrasound: The fundamentals, clinical applications and research trends. *Diagnostic and Interventional Imaging* **99**, 349–359 (2018).
50. Guex, A. G., Di Marzio, N., Eglin, D., Alini, M. & Serra, T. The waves that make the pattern: a review on acoustic manipulation in biomedical research. *Materials Today Bio* **10**, 100110 (2021).
51. Armagan, O., Bakilan, F., Ozgen, M., Mehmetoglu, O. & Oner, S. Effects of placebo-controlled continuous and pulsed ultrasound treatments on carpal tunnel syndrome: a randomized trial. *Clinics (Sao Paulo)* **69**, 524–528 (2014).
52. Fomenko, A., Neudorfer, C., Dallapiazza, R. F., Kalia, S. K. & Lozano, A. M. Low-intensity ultrasound neuromodulation: An overview of mechanisms and emerging human applications. *Brain Stimulation* **11**, 1209–1217 (2018).

53. Yu, K., Niu, X., Krook-Magnuson, E. & He, B. Intrinsic functional neuron-type selectivity of transcranial focused ultrasound neuromodulation. *Nat Commun* **12**, 2519 (2021).
54. King, R. L., Brown, J. R., Newsome, W. T. & Pauly, K. B. Effective Parameters for Ultrasound-Induced *In Vivo* Neurostimulation. *Ultrasound in Medicine & Biology* **39**, 312–331 (2013).
55. Yoo, S., Mittelstein, D. R., Hurt, R. C., Lacroix, J. & Shapiro, M. G. Focused ultrasound excites cortical neurons via mechanosensitive calcium accumulation and ion channel amplification. *Nat Commun* **13**, 493 (2022).
56. Sellani, G. *et al.* Assessing heating distribution by therapeutic ultrasound on bone phantoms and in vitro human samples using infrared thermography. *J Ther Ultrasound* **4**, 13 (2016).
57. Leong, T. S. H., Ashokkumar, M. & Kentish, S. THE FUNDAMENTALS OF POWER ULTRASOUND - A REVIEW. *Acoustics Australia* (2011).
58. Luan, S., Williams, I., Nikolic, K. & Constandinou, T. G. Neuromodulation: present and emerging methods. *Front Neuroeng* **7**, 27 (2014).
59. Beisteiner, R., Hallett, M. & Lozano, A. M. Ultrasound Neuromodulation as a New Brain Therapy. *Adv Sci (Weinh)* **10**, 2205634 (2023).
60. Zhang, T., Pan, N., Wang, Y., Liu, C. & Hu, S. Transcranial Focused Ultrasound Neuromodulation: A Review of the Excitatory and Inhibitory Effects on Brain Activity in Human and Animals. *Front Hum Neurosci* **15**, 749162 (2021).
61. Bennett, S. H., Kirby, A. J. & Finnerty, G. T. Rewiring the connectome: Evidence and effects. *Neurosci Biobehav Rev* **88**, 51–62 (2018).
62. Darmani, G. *et al.* Non-invasive transcranial ultrasound stimulation for neuromodulation. *Clinical Neurophysiology* **135**, 51–73 (2022).
63. Baron, C., Aubry, J.-F., Tanter, M., Meairs, S. & Fink, M. Simulation of intracranial acoustic fields in clinical trials of sonothrombolysis. *Ultrasound Med Biol* **35**, 1148–1158 (2009).
64. Kim, Y. H. *et al.* Patterned Interference Radiation Force for Transcranial Neuromodulation. *Ultrasound in Medicine & Biology* **48**, 497–511 (2022).
65. Kim, Y. H., Kim, J. N., Park, K. K., Firouzi, K. & Khuri-Yakub, B. T. Comparison of Waveform Modulation Methods Used in Pattern Interference Radiation Force Neuromodulator. in *2022 IEEE International Ultrasonics Symposium (IUS)* 1–4 (2022). doi:10.1109/IUS54386.2022.9957675.
66. Levario-Diaz, V., Bhaskar, P., Carmen Galan, M. & Barnes, A. C. Effect of acoustic standing waves on cellular viability and metabolic activity. *Sci Rep* **10**, 8493 (2020).
67. Menz, M. D. *et al.* Radiation Force as a Physical Mechanism for Ultrasonic Neurostimulation of the Ex Vivo Retina. *J. Neurosci.* **39**, 6251–6264 (2019).
68. Zhu, J. *et al.* The mechanosensitive ion channel Piezo1 contributes to ultrasound neuromodulation. *Proc Natl Acad Sci U S A* **120**, e2300291120 (2023).
69. Weinreb, E. & Moses, E. Mechanistic insights into ultrasonic neurostimulation of disconnected neurons using single short pulses. *Brain Stimulation* **15**, 769–779 (2022).

70. Kreß, S. *et al.* 3D Printing of Cell Culture Devices: Assessment and Prevention of the Cytotoxicity of Photopolymers for Stereolithography. *Materials (Basel)* **13**, 3011 (2020).
71. Li, G.-F. *et al.* Improved Anatomical Specificity of Non-invasive Neuro-stimulation by High Frequency (5 MHz) Ultrasound. *Sci Rep* **6**, 24738 (2016).
72. Wei, Z. *et al.* A comparison of neuronal population dynamics measured with calcium imaging and electrophysiology. *PLoS Comput Biol* **16**, e1008198 (2020).
73. Lagache, T., Hanson, A., Pérez-Ortega, J. E., Fairhall, A. & Yuste, R. Tracking calcium dynamics from individual neurons in behaving animals. *PLoS Comput Biol* **17**, e1009432 (2021).
74. Duchen, M. R. Mitochondria, calcium-dependent neuronal death and neurodegenerative disease. *Pflugers Arch* **464**, 111–121 (2012).
75. Harr, M. W. & Distelhorst, C. W. Apoptosis and Autophagy: Decoding Calcium Signals that Mediate Life or Death. *Cold Spring Harb Perspect Biol* **2**, a005579 (2010).